Chapter 3

Observations and Results

3.1 Introduction

This chapter presents the details of various observations that were made during the course of this thesis. The aims of the different observations, the telescopes used and the results obtained are described. The main aim of these observations was to study the low-density, partially ionized gas in the ISM starting from observations of low-frequency radio recombination lines of carbon. Observations were made using several telescopes - the low-frequency array at Gauribidanur, the Ooty radio telescope, the 10.4 m mm-wave telescope at RRI arid the Very Large Array of NRAO, Socorro, USA.

The observations made with the Gauribidanur radio telescope are central to the theme of the thesis. Carbon recombination lines in absorption near 34.5 MHz (corresponding to transitions near principal quantum number n $\sim$ 575) were observed with the telescope towards Cas A, the Galactic centre and several directions in the Galactic plane. These high-Rydberg state recombination lines of carbon arise in relatively cold interstellar clouds where carbon is ionized by background ultraviolet photons. Even at the low electron densities that prevail in these clouds (typically ≤ 0.1 cm^{-3}), pressure broadening effects are expected to be observable at 34.5 MHz.

These lines are expected to turn into ernission at frequencies above 200 MHz or so (Payne, Anantliaramaiali & Erickson 1989, hereafter PAE89) because of inversion of level populations which results in stimulated ernission. The ratio of the line strengths at low frequencies ($\nu < 100$ MHz) and at high frequencies ($\nu > 200$ MHz) can be used to place constraints on the physical conditions in the line-forming regions. The Ooty Radio Telescope which operates near 328 MHz was used to observe these lines in emission from several directions in the Galactic plane including the direction towards Cas A and the Galactic centre.

The directiou towards Cas A has been extensively studied in carbon recombination

lines, the HI 21-cm line and in molecular lines. However, the association of ionized carbon with other components of the ISM has not been firmly established. Typical model temperatures and densities obtained for CII regions do not provide conclusive evidence for association of these regions with either HI or molecular gas. Comparing the spatial distribution of ionized carbon as traced by recombination lines with that of atomic hydrogen and of molecular hydrogen could provide another clue for establishing the sites of origin of the low-frequency carbon lines. To compare the spatial distributions, the ionized gas across Cas A was imaged in C270α with the Very Large Array (VLA) and the molecular gas distribution across Cas A was mapped in ^{12}CO using the 10.4m mm-wave telescope at RRI. Published maps of the HI 21-cm line distribution were used for comparision with the atomic gas distribution.

One of the Galactic plane positions, G14+00 from which carbon recombination lines were detected, both at 34.5 MHz and 328 MHz was imaged at 330 MHz in C270α using the Very Large Array. The aim of this observations was to study the spatial extent of the line-forming region.

In addition to observing the very low-frequency carbon RRL from the partially ionized regions in the Galactic plane at low temperatures, we used the VLA to image relatively warmer partially ionized medium (PIM or H^{o}) associated with the HII regions of the W3 complex in 168α recombination lines near 20 cm. The distribution of the narrow hydrogen and carbon lines over W3A are compared. The line strengths are also modelled to obtain the physical conditions likely to exist in the PIM.

In this chapter, the various observations mentioned above are described. The observations are grouped in 4 sections corresponding to the four radio telescopes that were used i.e. the Gauribidanur radio telescope, the Ooty Radio telescope, the RRI 10.4m telescope and the Very Large Array. The observations towards W3 using the VLA are described separately in Chapter 6. Each section in this chapter is sub-divided into parts covering the astrophysical plan, some details of the instruments, the observations, the data reduction and finally the results. The interpretation of the results are presented in subsequent chapters.

3.2 Observations with the Gauribidanur Telescope

3.2.1 The Astrophysical Plan

In 1980, the first low-frequency recombination line in absorption was detected at 26.1 MHz against the strong radio continuum source, Cas A (Konovalenko & Sodin 1980). The line was shown to be due to a transition from n=631 to n=632 in Rydberg atoms

of carbon by Blake *et.al.* (1980). This direction has subsequently been observed in carbon recombination lines at frequencies ranging from 14 MHz to 1420 MHz and the data has been modelled to obtain the physical parameters of the line-emitting regions (PAE89, Payne, Anantharamaiah & Erickson 1994 (hereafter PAE94), Sorochenko & Walmsley 1991). At low frequencies, pressure and radiation broadenings are expected to produce a Voigt profile for the observed lines. Low signal-to-noise ratio, typical of spectra at low frequencies and the possible removal of a (wrong) baseline have prevented the detection of the weak Lorentzian wings in the expected Voigt profile and hence the correct estimate of the equivalent width of the profile. In the course of this thesis, we aimed to obtain a high signal-to-noise profile of the carbon recombination lines around n=575 towards Cas A and to detect the Lorentzian wings. This involved observing the direction towards Cas A over a long period of time using the Gauribidanur telescope operating at 34.5 MHz.

After the discovery and further successful observations of low-frequency carbon recombination lines towards Cas A, attempts were made to observe these lines in absorption towards other directions. Anantharamaiah *et.al.* (1988) used the 93m, 43m telescopes at Green Bank and the 300m telescope at Arecibo to search for lines in the Galactic plane. Only two further detections were made; towards M16 at 68 & 80 MHz and towards the Galactic centre at 75 MHz. Absorption lines of carbon at 25 MHz were successfully observed from the directions of NCG2024, G75+00, DR 21 and S 140 with the UTR-2 telescope in Ukraine by Konovalenko (1984) and Golynkin & Konovalenko (1990). Erickson, McConnell & Anantharnaiah (1995, hereafter EMA95) have observed the inner Galaxy in carbon recombination lines near 76 MHz ($n = 443$) using the Parkes radio telescope in Australia and detected carbon recombination lines in absorption from all the directions in the Galactic plane with $l < 20°$. This is an impressive result and points at the ubiquity of the cold, ionized carbon in the inner Galaxy, which is probably associated with the neutral hydrogen gas in the Galaxy. In the course of this thesis, we undertook to observe the Galactic plane in carbon recombination lines in absorption at 34.5, MHz with the Gauribidanur telescope. The main aim was to find out how widespread these lines are and to study the physical properties of the ionized carbon gas. The correlation of the ionized gas with other constituents of the ISM is also studied. A few sources observed in carbon RRL at frequencies near 25 MHz were also probed for carbon RRL at 34.5 MHz. The overall aim is to combine the results of the observations at 34.5 MHz with the results at other frequencies and obtain constraints on the properties of the gas responsible for the lines.

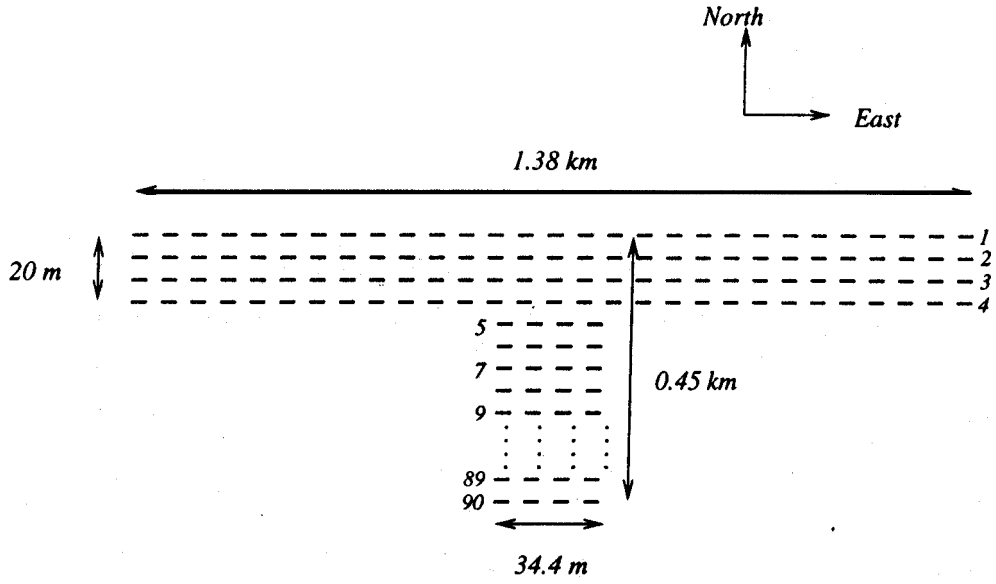

Figure 3.1 Schematic of the 'T'-array of dipoles at Gauribidanur - The four long dashed lines in the east-west direction represent the four rows of dipoles. The rows in the southern direction represent the 90 rows in that arm.

3.2.2 The Equipment

The Antenna:

The radio telescope at Gauribidanur (~ 80 km north of Bangalore; latitude = 13° 36' 12", longitude = 77° 26' 07") used for these observations is a 'T'-shaped array (Fig 3.1 & 3.2) of 1000 wide-band dipoles, each $\frac{3}{4}\lambda$ (λ = 8.7 m) long (Deshpande *et.al.* 1989 and references therein). The dipoles are oriented east-west (EW) and are sensitive to a 10-MHz band centred at 32 MHz. The actual observing band, determined by the preamplifiers, is 34.5 ± 1 MHz. The EW arm is 1.38 km long, from the centre of which a 0.45-km-long arm extends southwards, giving an aerial appearance of a 'T'-shaped aperture. The EW arm consists of 640 dipoles arranged in four rows of 160 dipoles each. Each row is separated by 5 m in the north-south (NS) direction. The total power half-power beamwidth (HPBW) of the EW arm is $\alpha \times \delta = 21' \times 25°\sec(Z)$ (where Z is the zenith angle) at $\lambda = 8.7$ m. The south arm consists of 360 dipoles arranged in 90 rows and has a total power beam width of $\alpha \times \delta = 14.5'' \times 69' \sec(Z)$. Only the EW arm was used for these observations.

The EW arm consists of 10 groups, each consisting of 64 dipoles combined in a Christmas-tree configuration. The outputs from the five groups each in the east and the west are combined separately with equal amplification, and brought to the receiver room through equal-length RF cables. Amplifiers in the signal path compensate for

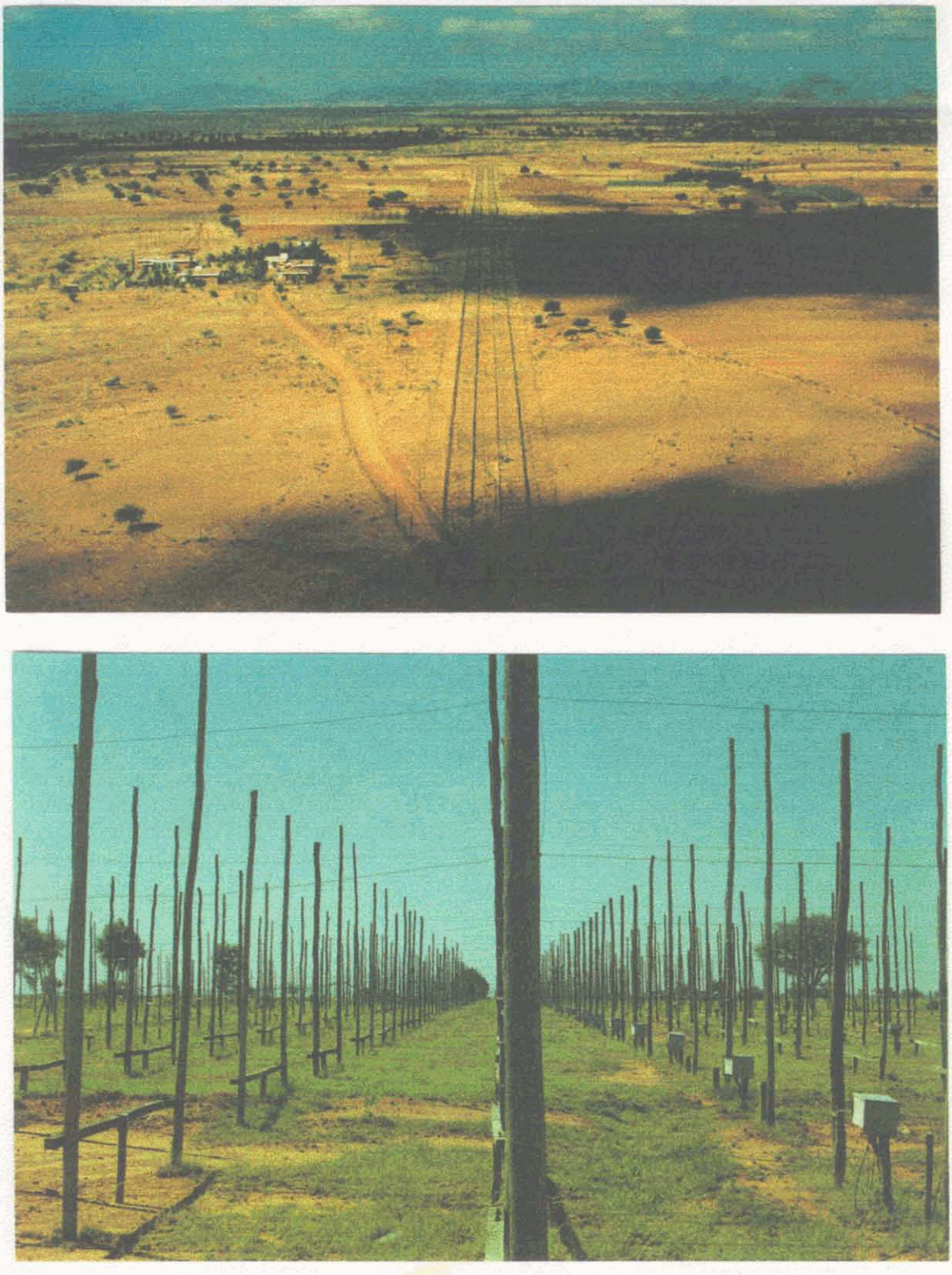

Figure 3.2 The picture on the top shows an aerial view of the sprawling Gauribidanur radii telescope. The shadow of a cloud is obscuring the central part of the telescope. The eastern arm of the telescope extends out of the photo towards us and the end is also obscured by the shadow of a doud. The south arm runs behind the cluster of buildings (which includes the observatory) and trees seen in the left of the centre. The picture on the bottom shows a dose-up of the array. The dipoles are fixed using wooden poles. The white boxes between the poles contain the amplifier and phase shifter circuits

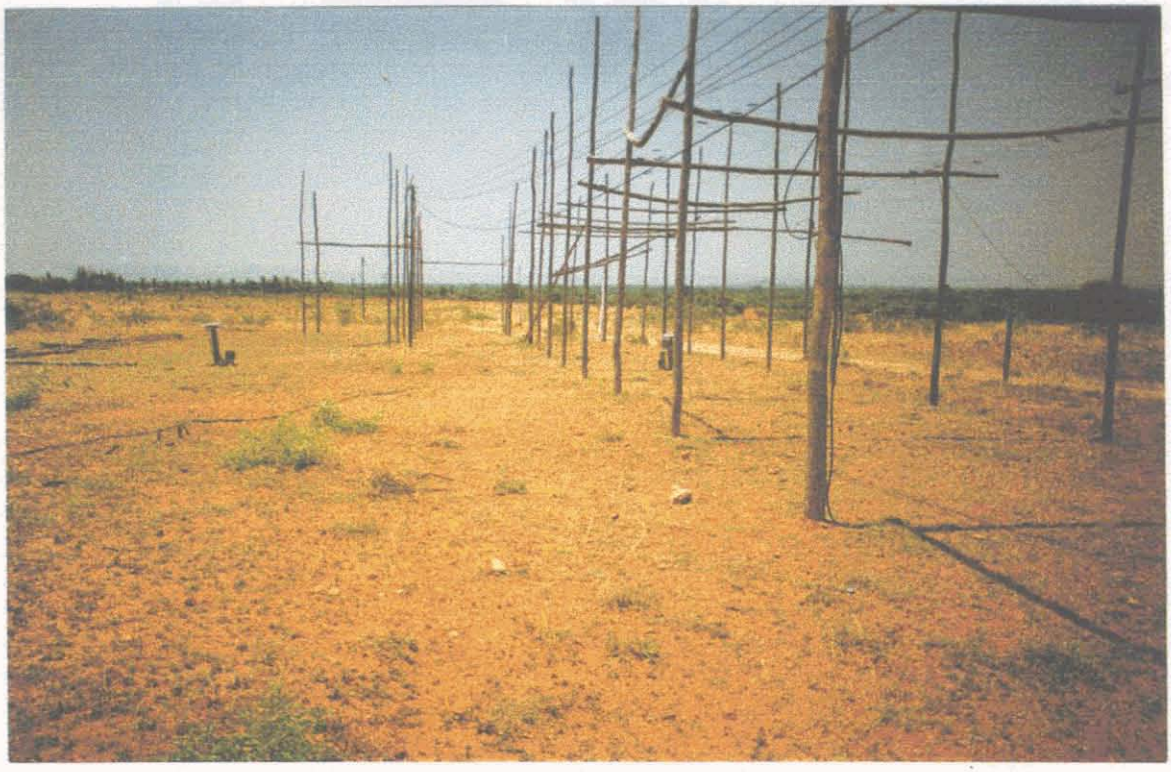

Figure 3.3 The fury of Mother Nature and low-frequency radio telescopes! A wild storm with intense lightning, strong winds and heavy rains swept through Gauribiianur on the 30th May 1995. It left behind a trail of destruction as demonstrated by these two photographs. The last section of the east arm is shown hare. A lone amplifier box stands in the midst of uprooted poles and hanging dipole wires. This damage was subsequently repaired by the observatory team at Gauribianur and the telescope was made as picture perfect as in Fig 3.2.

the cable losses. The EW arm has an effective area of about 12000 m^2 at zenith. The telescope is essentially a meridian transit instrument with only a minimal tracking capability. The telescope can be electrically steered to any declination in the range from $-45°$ to $75°$ in steps of $0.2°$ and any source in this declination range can be tracked for a duration of $42^m \sec\delta$ about transit time.

The Continuum Receiver:.

The continuum receiver is an analog system which can be used either in the correlation mode (ExW or $(E+W)\times S$) or in the total power mode ($(E+W)^2$ or $(E+W+S)^2$) (Deshpande 1987). The continuum receiver played an important role in our observations. As the output of the receiver could be displayed either on a chart recorder or a computer screen with an appropriate interface, it was used for equalizing the phases of the E and W arms from visual inspection of the power pattern of the antenna traced by the motion of a point source through the beam. Furthermore, since the line receiver used for these observations was a one-bit system which measured only a normalized power spectrum, a separate total power measurement was required for amplitude calibration. The continuum receiver provided this measurement.

A block diagram of the continuum receiver is shown in Fig 3.4. In the continuum receiver, the RF signals at 34.5 MHz from any two arms of the antenna are amplified and power-divided. One set of signals from both the arms are added to obtain a E+W or $(E+W)+S$ signal. Either the signals from the individual arm (for correlation mode) or the combined signal (for total power mode) are used in subsequent processing, as shown in Fig 3.4. The two signals are separately mixed with a 46-MHz local oscillator and down-converted to a 30-kHz band centred about an intermediate frequency of 11.5 MHz. A 1-kHz phase switch is provided to minimize stray pickup in the circuit. The two IF signals are then correlated and synchronously detected. The detected signal is digitized using an A/D convertor and read out by a personal computer (PC). The PC also displays the total power or correlator output of the receiver on its screen in the form of a graph. A variable attenuator connected in the RF path was used to calibrate the strength of the source with respect to a reference position. The brightness temperature of the reference position, which was generally chosen to be a direction free of discrete sources, was found from continuum maps at 34.5 MHz (Dwarakanath 1989) or by scaling from the maps at 408 MHz (Haslam *et.al.* , 1982).

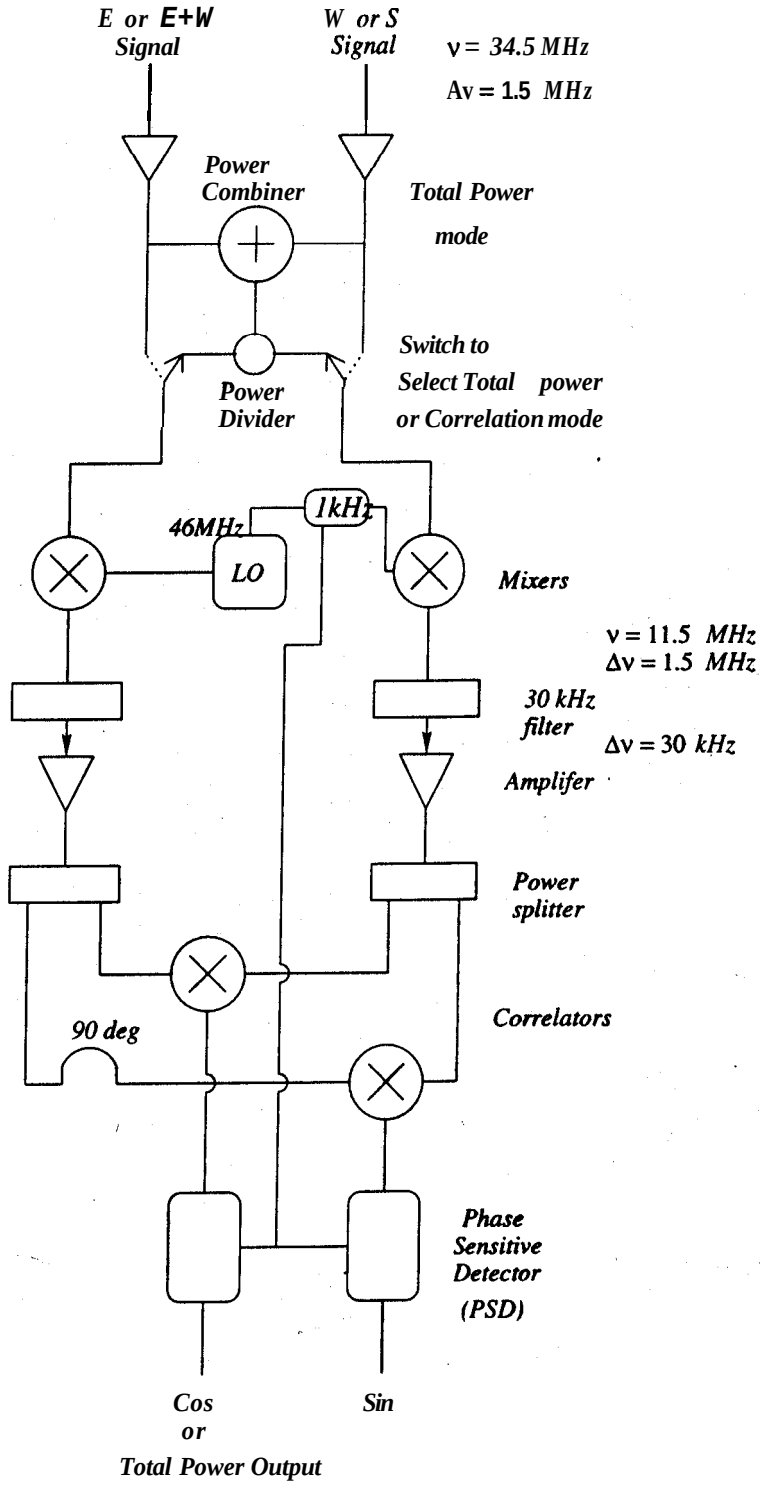

Figure 3.4 Block Diagram of the Continuum Receiver at Gauribidanur

The Line Receiver:

As mentioned previously, the Gauribidanur telescope is a meridian transit instrument with limited tracking ability ($\sim 42 \sec\delta$ minutes). The strongest known low-frequency carbon recombination line is towards the radio source, Cas A and the expected ratio of the line to continuum strength near 34.5 MHz towards this direction is $\sim 3.0 \times 10^{-3}$. Since Cas A could be observed only for 80 minutes a day with the Gauribidanur telescope, it would have taken a week to detect the expected absorption line with a signal-to-noise ratio of ~ 5. Directions in the Galactic Plane from where the lines are probably weaker would require weeks of observations. To make these observations less time-consuming, several adjacent transitions in the Rydberg atom are observed simultaneously and then averaged incoherently. As the physics of the adjacent transitions in a Rydberg atom are not expected to change drastically, averaging the adjacent transitions to effectively increase the integration time is justified. The line receiver at Gauribidanur was specially designed to simultaneously observe eight RRL transitions around $n \sim 575$. The 1.5-MHz observing band, determined by the front end amplifiers, contain 11 successive α (An = 1) transitions around n=575. The successive transitions are separated by approximately 180 kHz. Eight of these transitions which were relatively interference-free were selected for processing through the eight-line receiver.

A simplified block diagram of the spectral line receiver used for carbon RRL observations at 34.5 MHz with the Gauribidanur telescope is shown in Fig 3.5.

In the line receiver, the E+W and S (if used) signals from the array first enter the signal combiner unit. The signal combiner is designed to combine the E+W signal and the S signal with appropriate attenuation. It can also replace the signal from the telescope by noise generated by an in-built noise diode or can optionally add an external Continuous Wave (CW) signal with noise signal. The selection of the required output is done using a RF switch. This unit was useful for testing purposes in which noise was injected into the system along with a CW.

The output from the signal combiner is amplified and passed through a bandpass filter ($\Delta\nu \sim 3$ MHz) centred at 34.5 MHz. The signal is then mixed with an adjustable first local oscillator (LO1) at a frequency near 30.5 MHz and down-converted to an intermediate frequency (IF) of 4 MHz. The frequency of LO1 can be varied with a least count of 500 Hz. Any required radial velocity correction to the rest frequency is incorporated in this local oscillator. The down-converted first IF signal is amplified arid divided into eight equal parts required for subsequent processing in the eight-line receiver. These then pass through eight low-pass filters (LPF) of 8 MHz bandwidth

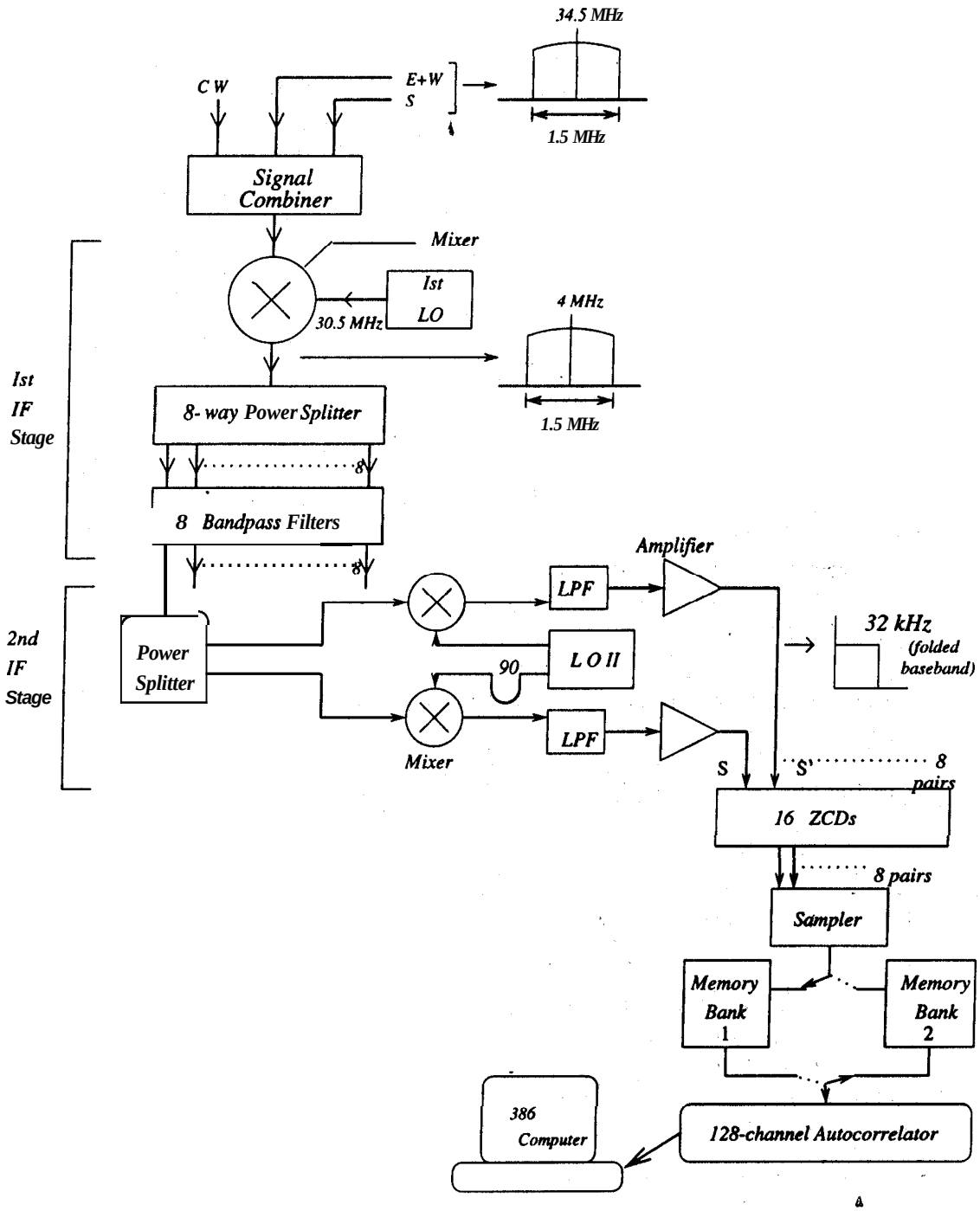

Figure **3.5 Block diagram of the eight-line receiver used for carbon recombination line observations near 34.5 MHz at Gauribidanur**

Table 3.1 a Lines observed using the eight-line Receiver at Gauribidanur

No.	Transition	Rest Frequency	2nd Local Oscillator Frequencies
1	C571α	35.248158	4.73388
2	C572α	35.063774	4.54823
3	C573α	34.880673	4.36512
4	C574α	34.698845	4.18325
5	C575α	34.518279	4.00272
6	C576α	34.338964	3.82336
7	C577α	34.160888	3.64526'
8	C579α	33.808453	3.29270

which remove any unwanted higher frequencies. This section constitutes the first IF stage.

In the second IF stage, the eight identical outputs from the first stage are further down-converted to 32-kHz basebands using eight different local oscillators. The second LOs are crystal oscillators generating CW signals at frequencies around 4 MHz at intervals of 180 kHz so that the eight line frequencies are made to appear in the eight 32-kHz basebands. The eight line frequencies, the corresponding quantum numbers and the second local oscillator frequencies are listed in Table 3.1. In this frequency conversion, the upper and lower side-bands are folded. A Double Side-Band (DSB) technique described by Radhakrishnan *et.al.* (1972) is used to separate the two side-bands. Each of the eight second LO signals are split into two and each pair is processed as follows. One LO signal is directly mixed with the first IF. We call this LO as the in-phase LO and the down-converted 2nd IF signal as the in-phase IF. The other LO signal is passed through a 90° phase shift and then mixed with the first IF signal. This we refer to as the quadrature-phase LO and the 2nd IF as the quadrature-phase IF. Hence for each 32-kHz band, a pair of second IF bands are obtained. These are designated as S (in-phase second IF) and S' (quadrature-phase second IF). These are required for separating the side-bands in the DSB system. The signals are then passed through eight 32-kHz low-pass filters and amplified before entering the digitization and sampling modules.

A one-bit digitization using zero cross detectors (ZCD) is employed at Gauribidanur. In one-bit digitization, the amplitude information of the signal is lost since only the sign

of the signal is recorded. One-bitting of data leads to increase in the noise by a factor of $\pi/2$. This increase is mainly due to power appearing in the harmonics of the signal. The reduction in the signal-to-noise ratio can be partially compensated by oversampling the data. In the sampler at Gauribidanur, the one-bitted data is sampled at twice the Nyquist rate of 64 kHz *i.e.* 128 kHz. Oversampling by a factor of two improves the signal-to-noise ratio by a factor of 1.17 *i.e.* decreases the noise by a factor of 0.85. The combined effect of one-bit sampling and oversampling leads to an effective increase in the noise by a factor of 1.34. In return, one gains a considerable simplification of the hardware. The one-bit sampled data is then autocorrelated.

The 128-channel, one-bit correlator (Ravindra 1983, Udayashankar 1986) was originally built for continuum observations in which an "all-sky" map was made by correlating the outputs of the EW arm with each of the 90 rows in the south arm of the array (Dwarakanath 1989). The correlator also has an autocorrelation mode of operation. If S and S' are the in-phase and quadrature-phase undelayed second IF signals and $S(\tau)$ and $S'(\tau)$ are the delayed versions of the same, then the complex autocorrelation functions in a DSB system are given by,

$$R_c(\tau) = S \times S(\tau) + S' \times S'(\tau) \quad (3.1)$$

$$R_s(\tau) = S \times S'(\tau) - S' \times S(\tau) \quad (3.2)$$

We refer to $R_c(\tau)$ and $R_s(\tau)$ as the cosine and sine parts of the autocorrelation function. The cosine Fourier transform of $R_c(\tau)$ gives the sum of the sidebands, U+L (U - Upper side-band and L - Lower sideband). The sine transform of the sine part of the autocorrelation function gives the difference spectrum, U-L (Radhakrishnan *et.al.* 1972, Udayashankar 1986). In line observations, the latter is important as it directly gives the difference spectrum. The two sidebands can be separated using the sum & differences which are obtained (*i.e.* U+L & U-L). The 128-channel autocorrelator which operates at a maximum speed of 2 MHz was used to process the signals corresponding to all the eight lines. The low sampling rate (128 kHz) of the basebands (32-kHz) enabled sequential processing of all the eight bands in the same autocorrelator when it was operated at a speed of 1 MHz. This required temporary storage of the line data which was provided by two 32 kB x 8-bit memory chips. The one-bit data of all the eight lines were written into one of these memory banks in 128 ms whereas the autocorrelator read and processed the stored data from the other memory bank at a rate of 1 MHz at the same time. As the data was sampled at twice the Nyquist rate (128 kHz), only alternate samples were autocorrelated as shown in Fig 3.6. The schematic of the correlator to obtain the cosine correlation, $R_c(\tau)$ is shown in Fig 3.7.

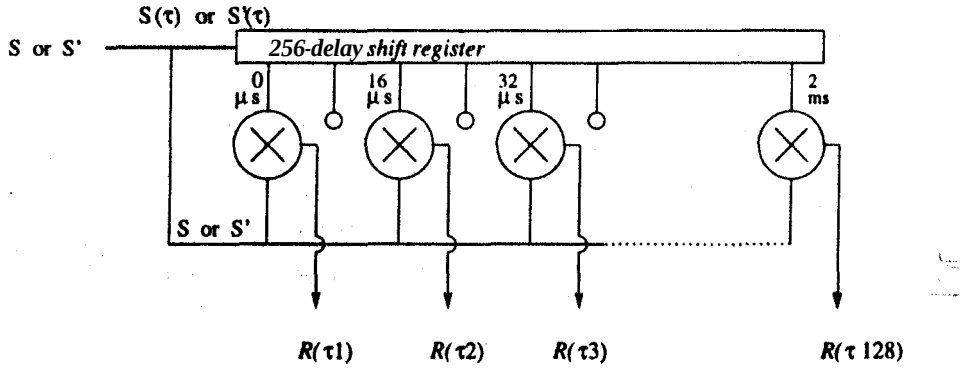

Figure 3.6 The 128-channel autocorrelator at Gauribidanur.

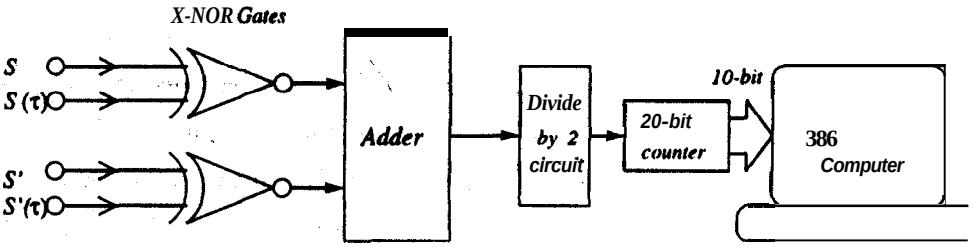

Figure 3.7 **Schematic of the Correlator used to obtain the cosine correlation, $R_c(\tau)$**

X-NOR and X-OR logical gates function **as** the multipliers. The multiplied outputs are added to obtain the correlations given by Eqn (3.1) and **Eqn** (3.2). The operations are as given below:

$$R_c(\tau) = \frac{1}{2}\,(XNOR(S, S(\tau)) + XNOR(S', S'(\tau))) \tag{3.3}$$

$$R_s(\tau) = \frac{1}{2}\,(XNOR(S, S'(\tau)) + XOR(S', S(\tau))) \tag{3.4}$$

where S and S' are the in-phase and quadrature-phase undelayed samples and S(τ) and S'(τ) are the corresponding delayed samples **as** mentioned above. The delayed data train is obtained using a 256-delay shift register as shown in Fig 3.6. The minimum lag in the shift register is 8 ps and it is increased in steps of this minimum delay to obtain the maximum lag, τ_{max} of 2 ms. Although the shift register generates 256 delayed versions, only the alternate delayed signals (*i.e.* 128 delays of 16 ps) are actually correlated as shown in Fig 3.6. Due to the truncation of the autocorrelation function with a rectangular window function extending **upto** a delay of τ_{max}, the spectral resolution in the power spectrum (which is obtained from the Fourier transform of the autocorrelation function) is given by $0.605/\tau_{max}$, which in our case is 302.5 Hz (2.6 kms^{-1}). The resolution after **hanning** smoothing is $1/\tau_{max}$ ie 500 Hz (4.4 kms^{-1}).

As each autocorrelation function is a combination of two logical operations (Eqn 3.3

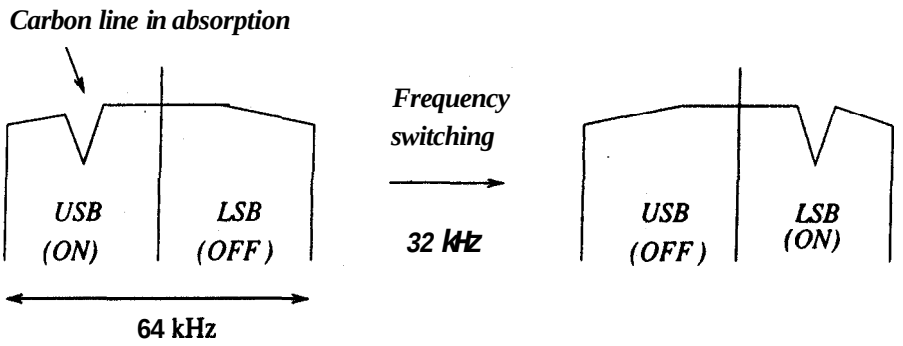

Figure 3.8 **Switching the first LO frequency to measure the reference spectrum.**

& Eqn 3.4), the number of multipliers required by a DSB system.is twice the number of autocorrelation lags. There are thus, 256 cosine and sine multipliers in the DSB system and it gives 128 cosine and 128 sine correlations. The autocorrelation counts are integrated in 20-bit counters for a pre-integration time of 128 ms. At the end of this period, each of the 256 counters send a 14-bit number to the the PC-based data acquisition system (DAS). The DAS reads in only the 10 most significant bits as the remaining four bits represent noise.

Data Acquisition

The Data Acquisition System (DAS) consists of both hardware and software parts. The hardware consists of an interface between the autocorrelator and the computer which reads the data and stores it. There is also a hardware interface between the computer and the declination-setting, tracking system and the first LO switching system.

The declination and tracking phase shifters on the field are controlled by a tracking module in the receiver room which is controlled by the PC. The first LO frequency is switched by 32 kHz every two seconds such that the spectral line shifts from the upper side-band to the lower side-band as shown in Fig (3.8). The side-band in which the line appears is referred to as the 'ON' band and the bther side-band as the 'OFF' band. The ON and OFF states of the side-bands are thus swapped every 2 seconds. The end-effect is similar to dual-Dicke switching in which the reference spectrum is measured at the same time as the source spectrum. This type of frequency switching avoids losing time on the source when the reference spectrum is being measured. Hence over any given time interval, half the time the line is in the upper side-band (USB) and half the time it is in the lower side-band (LSB). The line data is integrated in the random access memory of the PC for 30 seconds after which the data is written out to the hard disk.

The DAS assigns a weight to each channel of the correlator. The channel weight is the total number of times that channel shows a 'healthy' count during the pre-integration. At the end of the pre-integration time, the channel weights are also written out into the disk along with the correlation counts.

Some online editing of the data is done by the DAS. The 10-bit number sent by the autocorrelator to the PC could have any value between 0 and 1023. Here 0 counts corresponds to anti-correlation, 512 to zero-correlation and 1023 to total correlation. Since the basebands have roughly a rectangular shape, we expect the correlation to drop to zero (*i.e.* a value of 512) after the first few channels in the lag-domain. Occasionally, we found that a few correlators misbehaved and the counts recorded were either 384, 256 or 0 instead of $\sim$ 512. These 'spike-like' features in the correlation domain gave rise to a ringing effect in the spectral domain. Hence it was important to remove the 'spiky' channels. Such faulty channels in the acquired data were checked by the DAS and if a channel was found to be faulty, it was discarded and the channel weight was not incremented. Another problem was that the self-correlation count used to drift away from 1023. If this was found to be the case then the entire spectrum was discarded. A new data file was created on the disk every 9 minutes. Each file contained records of the correlation counts and channel weights for each of the eight lines with a pre-integration time of 30 seconds.

Technical Problems: Low-frequency observational radio astronomy is subject to a multitude of problems. Owing to the large physical dimensions of the telsecope, much maintenance work is required to keep it functioning. Some of the problems that were particular to the Gauribidanur telescope are listed below:

- Man-made interference in the form of wireless radio transmission and personal computers in the receiver room was the major problem which generally restricted the observing to night times. A strong external interference spike at 33.7921 MHz always corrupted one of the eight bands.
- Phasing of the dipoles and wire-continuity decks had to be regularly made on the sprawling array.
- Lightning has the potential to cause large-scale damage to the array. We had to replace a large number of pre-amplifiers damaged in a lightning strike during the course of this thesis. Moreover, on May 30 1995, a storm swept through Gauribidanur and left behind a trail of destruction (See Fig 3.3. Many wooden poles were uprooted, dipole wires were cut, transformers were destroyed and

amplifiers blew. Amplifiers and the phase-shifter modules were rained on and shorted. It took close to two months to get the EW arm back into operation.

Offline Data Reduction

The data acquired by the acquisition computer was then transferred to a workstation for further processing. A software package specially developed for this project was used for the initial steps in the data analysis. The main functions are listed below.

- Read in raw data files containing autocorrelation counts integrated for 30 seconds.
- Normalize the correlations using the "channel weights" and calculate the digital correlation coefficient, ρ_d. The channel weights were important in the subsequent stages of analysis when individual channels had to be edited due to interference.
- Replace a few faulty correlation channels by the average of its neighbouring channels. About 4 % of the total channels had to be thus replaced.
- Apply Van Vleck correction to the one-bitted digital correlation coefficient to obtain the analog correlation coefficient, ρ_a.

$$\rho_a = sin(\frac{\pi}{2}\rho_d) \tag{3.5}$$

- Fourier transform the autocorrelation function to obtain the power spectrum.
- Calculate the difference spectrum, $\frac{ON-OFF}{OFF}$. Two difference spectra were made corresponding to $\frac{ON_{USB}-OFF_{USB}}{OFF_{USB}}$ and $\frac{ON_{LSB}-OFF_{LSB}}{OFF_{LSB}}$
- Hanning smooth the difference spectrum to a coarser resolution of 4.4 kms^{-1}.
- Calculate the expected rms noise on the spectrum and then flag any data which is not within a user-specified range in terms of this rms noise. The flagging was done by assigning zero weights to the bad channels. The typical cutoff used was $\pm 5\sigma$. If more than 20 channels in the spectrum were found to have values outside this range, then the entire spectrum was discarded.
- Average the edited data of eight lines contained within a single raw data file to produce a single set of eight integrated spectra separately for the USB and the LSB (*i.e.* totally 16 spectra). Write out the averaged data in an output file with proper header, data and channel weights.

This constitutes the first stage of off-line data analysis. In the second stage,

- many such averaged spectra (which on the average had four minutes of integration) are processed.
- A linear baseline is removed from all the 4-minute spectra and the rnis noise on each epectrum is calculated. Data which are affected by interference are discarded by blindly flagging data outside a safe range of $\pm 6\sigma$.
- Interactive editing is possible at this stage. Channels or entire spectrum which are affected by interference and which have not been removed in the first stage can be edited out.
- Once all the data are visually examined and edited, the 4-minute spectra for all the eight lines were separately averaged with proper channel weighting. These are the final spectra for the eight lines. All through this analysis, the channel weights are updated and maintained.

In the third and last stage of data reduction, the NRAO spectral line reduction package, UniPOPS was used for the final averaging of the eight lines. The line data were first converted to the UniPOPS scan format which consists of extensive header information in addition to the data. At this point, the channel weights were riot considered. Instead, an average integration time from these channel weights was derived and assigned to each spectrum. The data were again examined in UniPOPS for the presence of weak interference which may have escaped notice in the earlier analysis stages. In UniPOPS, the 16 spectra were combined after applying weighting proportional to their integration times to obtain the final spectrum towards the source.

3.2.3 The Observations

Observations of carbon RRL using the Gauribidanur telescope were carried out in two observing sessions: June - October 1994 and July - October 1995. In both the sessions, several positions in the Galactic Plane and some lines-of-sight towards a few specific sources were observed. The list of sources observed, their coordinates, the radial velocity settings, effective integration time and the rnis noise in the spectra are listed in Table 3.2. The main aim of these observations was to observe several directions in the Galactic plane in carbon recombination lines at 34.5 MHz. The choice of the directions in the Galaxy did riot follow any strict physical criteria except that the Galactic non-thermal background is stronger in the inner Galaxy and hence if ionized carbon exists throughout the Galaxy then it was more likely to be observable in absorption in the inner Galaxy. Observations were generally made at Galactic latitude. $b = 0°$ and

Table 3.2 **List of Sources that were searched for Carbon Lines near 34.5 MHz.**

No.	Position	α(1950) hh mm ss	δ(1950) dd mm ss	V_{lsr} setting kms^{-1}	$\frac{\Delta T_{rms}}{T_{sys}}$ 10^3	Effec Time hours
1	G342+00	16 50 34	-43 37 38	-20.0	0.35	63.5
2	G352+00	17 21 47	-35 37 25	-20.0	0.20	95.3
3	G00+00	17 42 27	-28 55 00	0.0	0.20	58.7
4	G05+00	17 54 00	-24 37 59	0.0	0.23	70.3
5	G10+00	18 04 47	-20 17 51	0.0	0.20	91.3
6	G14+00	18 12 59	-16 48 00	20.0	0.22	55.0
7	G16.5+00	18 17 57	-14 36 18	25.0	0.22	68.3
8	G25+00	18 34 12	-7 05 51	45.0	0.23	78.3
9	G45.2+00	191144	104850	20.0	0.23	45.8
10	G50+00	19 21 02	15 02 41	25.0	0.27	108.0
11	G55+00	19 31 08	19 25 32	25.0	0.23	50.7
12	G63+00	19 48 31	26 21 12	20.0	0.19	72.0
13	G75+00	20 19 02	36 26 46	0.0	0.15	188.0
14	G81+00	203717	411658	25.0	0.31	114.0
15	G85+00	20 23 08	21 22 05	25.0	0.34	41.7
16	G97+00	21 42 21	52 56 10	-20.0	0.29	91.5
17	G99+00	215247	541159	-20.0	0.33	169.5
18	G100+00	21 58 15	54 48 34	-20.0	0.20	178.3
19	G125+00	01 06 22	62 31 58	-20.0	0.37	88.8
20	G130+00	01 48 45	61 47 14	-20.0	0.37	128.5
21	G145+00	03 34 08	55 24 12	-20.0	0.37	100.0
22	S 140	221736	630400	-20.0	0.39	24.3
23	DR 21	20 37 13	42 09 00	0.0	0.35	28.3
24	Orion	05 32 48	-05 27 00	0.0	0.54	19.7
25	Cygnus Loop	20 49 30	29 50 00	25.0	0.16	99.8
26	Cygnus A	195745	403600	0.0	0.23	62.3
27	W3	02 21 50	61 53 20	-50.0	0.39	238.8
28	W49	190851	090227	60.0	0.46	42.9
29	W51	192017	140201	50.0	0.20	69.0
30	G203.1+2.1	06 38 17	09 43 20	8.0	0.5	12.0
31	G224.6-2.4	070156	-11 23 55	15.0	0.22	49.1
32	Rosette Nebula	062918	045700	0.0	0.34	37.5
33	Cas A	23 21 11	58 33 48	-50.0	0.15	423.5

In columns 6 & 7, the rms noise $\Delta T_{rms}/T_{sys}$ and the effective integration time on the source have been listed.

towards more number of directions in the inner Galaxy. The selection was constrained by the transit nature of the telescope and the need for obtaining long integration times towards each direction. The types of sources that were chosen were directions at different longitudes in the Galactic plane, specific sources like W49, W51 and sources where low-frequency (25 MHz) lines had been observed previously in absorption like S 140, DR 21 (Golynkin & Konovalenko 1990) and Cas A (references in PAE94). The target noise level was set to $\Delta T_{rms}/T_{sys} = 2.5 \times 10^{-4}$ which was achievable if each direction was observed for 10 hours of telescope time and if six of the eight lines could be averaged. A noise level of $\Delta T_{rms}/T_{sys} \sim 3 \times 10^{-4}$ was achieved on the average. To check the receiver stability and sensitivity that could be achieved, signal from a noise source was injected into the entire receiver system and the data was integrated for a long time. After averaging all the data, it was possible to attain a noise level of $\Delta T_{rms}/T_{sys} = 1 \times 10^{-4}$. The observations were restricted to night-time because of severe interference hampering them during the day-time. Another constraint arose from the transit nature of the telescope which restricted the total time that a source could be observed at a stretch, to $42 \sec\delta$. Hence, in a typical observing session from 2200 to 0700 local time, on the average, seven sources could be observed. Generally each position had to be observed for 10 nights to achieve the required sensitivity.

During the observing run in 1994, we observed about 50 directions in the Galactic plane. Unfortunately most of these directions were observed for only five days and hence the spectra had poor signal-to-noise ratio. The $\Delta T_{rms}/T_{sys}$ in most of the spectra was only 5×10^{-4}. Moreover, we realized that the declination-setting and tracking phase shifters were not functioning properly which cast doubts on telescope pointing. Owing to doubts regarding the quality of this data we decided not to use these data.

In the observing session of 1995, the 34 directions noted in Table 3.2 were observed. Each of these directions was observed for about 10 hours of telescope time. On the average, six out of the total eight bands which were processed by the eight-line receiver were free of interference and hence usable. A typical observation of a direction proceeded as follows: The observation started with the calibration measurement using the continuum receiver. The increase in the system temperature due to the programme source was measured with respect to a reference position in the sky which was relatively free of strong radio sources as seen in the 34.5 MHz sky map (Dwarakanath 1989). The two 1st LO frequencies separated by the switching interval of 32 kHz were set. In principle, a DSB system does not require frequency switching because it simultaneously measures both the signal spectrum (referred to as ON) and the reference spectrum (referred to as OFF). In practise, however, we found that the difference spectrum thus obtained had

baseline problems. To remove this, frequency switching between the two side-bands as shown in Fig 3.8 was employed. The 1st LO frequency was switched every 2 seconds so that the line frequency alternated between the two side-bands. This enabled us to use the USB 'OFF' spectrum to correct the frequency response of the USB 'ON' spectrum and likewise in the case of the LSB. This technique resulted in excellent baselines for the two sidebands and only linear baselines had to be removed in subsequent processing. The data acquisition was started when the source entered the telescope beam and data was recorded in the PC till the source reached the extreme position of the tracking beam.

3.2.4 The Results

Out of the total 34 positions observed with the Gauribidanur radio telescope, carbon recombination lines were detected from 10 directions. As expected at this frequency, all the detected lines are in absorption. A high signal-to-noise ratio spectrum was obtained towards Cas A and the line profile is shown in Fig 3.9. The absorption spectra obtained towards the other nine directions are shown in Fig 3.10. The peak line-to-continuum ratio observed towards these directions is of the order of a few times 10^{-4} as listed in Table 3.3. The rest of the positions do not show a clear detection to a 5a limit of 5.0 x 10^{-4}. The spectra observed towards these directions are shown in Fig 3.11. In almost all the cases, only a linear baseline had to be removed to obtain these final spectra. The effective integration time on each source was, on the average, more than 50 hours.

The results of the carbon lines observed towards Cas A, the Galactic Centre and other directions are described in more detail below:

Cas A: A high signal-to-noise ratio spectrum was obtained towards the direction of Cas A which is shown in Fig 3.9. More than 400 hours of data has been averaged in this spectrum. The peak lineto-continuum ratio is 3.7 x 10^{-3}. This is equivalent to the optical depth of the carbon-line forming gas in front of Cas A. In obtaining the spectrum shown in Fig 3.9, only a linear baseline had to be removed from the final spectrum. The absorption profile clearly displays weak, broad wings which we interpret as evidence for pressure or/and radiation broadening. This is the first time that the Lorentzian wings of a pressure or radiation broadened low-frequency carbon recombination line profile have been clearly detected.

In the direction of Cas A, molecular line spectra show the presence of three components: components at -47 kms^{-1} and -39 kms^{-1} due to the gas in the Perseus arm and

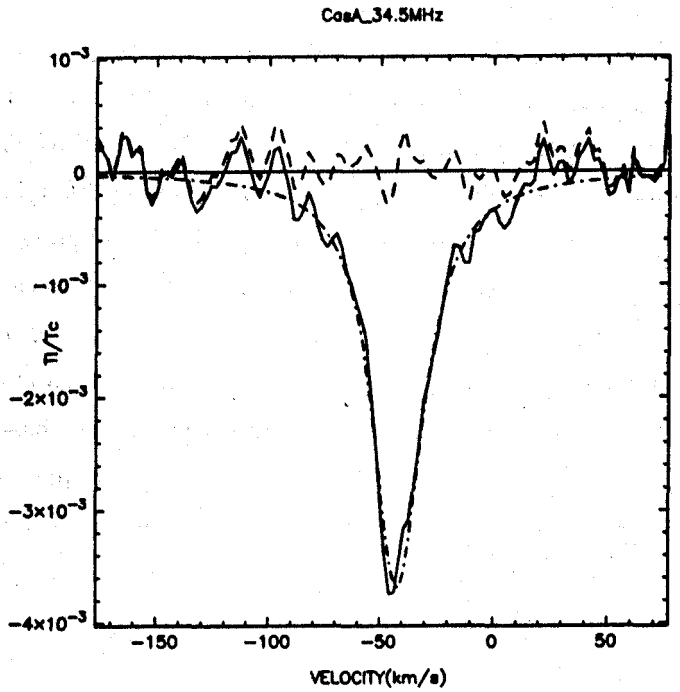

Figure 3.9 Spectrum Towards Cas A at 34.5 MHz. The solid line is the observed spectrum, the dash-dotted line is a single-component Voigt fit to the observed profile and the dashed line represents the residuals after the fit is removed from the observed profile. The fit parameters are $T_l/T_{sys}=-3.7(0.1) \times 10^{-3}$, $V_{lsr} = -42.0(0.3)$ kms^{-1}, Doppler FWHM = 5(0.3) kms^{-1}and Lorentzian FWHM = 26(0.6) kms^{-1}.

one component at 0 kms^{-1}due to the gas in the Orion arm. The high-frequency (> 200 MHz) carbon recombination lines observed in emission towards this direction also show the presence of the three components (PAE89). In the case of the low-frequency (< 150 MHz) lines observed towards Cas A, pressure and radiation broadening, both of which are strong functions of the principal quantum number, start becoming significant, causing the Perseus arm features to merge into a single component. This is clearly seen in the carbon line observations at frequencies ranging from 34 to 328 MHz which have been discussed in PAE89. In our spectrum near 34.5 MHz also, the two Perseus arm components are merged into a single component appearing at -42 kms^{-1}. There is a slight asymmetry in the profile near 0 kms^{-1}, probably caused by the feature due to

the gas in the Orion arm, but it is not sufficiently strong to enable identification as a separate feature.

In Fig 3.9, a single-component Voigt-shaped profile (dash-dotted line) has been superposed on the observed profile (solid line). The dashed line represents the residuals after removing the fit from the observed profile. Doppler width of 5 kms^{-1} was determined from the line that we detected at a higher frequency (328 MHz) at which pressure or radiation broadening is negligible. Other high frequency lines that have been detected towards Cas A also give a similar value for Doppler-broadening (PAE89). A peak optical depth of 3.7 $\times 10^{-3}$ with a Lorentzian width of 26 kms^{-1} gave a reasonably good fit to the observed profile as shown in the figure. We were also able to obtain a two-component fit centred at velocities of -44 kms−'and -38 kms^{-1} with Doppler widths of 5 kms^{-1} and Lorentzian widths of 25 kms^{-1}, to the spectral line observed towards Cas A. However, to allow consistent modelling with other low-frequency carbon recombination line observations we use only the single-component fit to the profile. The spectrum has a rms noise of $\Delta T_{rms}/T_{sys} \sim 1.5 \times 10^{-4}$, the lowest that we achieved in the entire observing session. This detection is further discussed in Chapter Four.

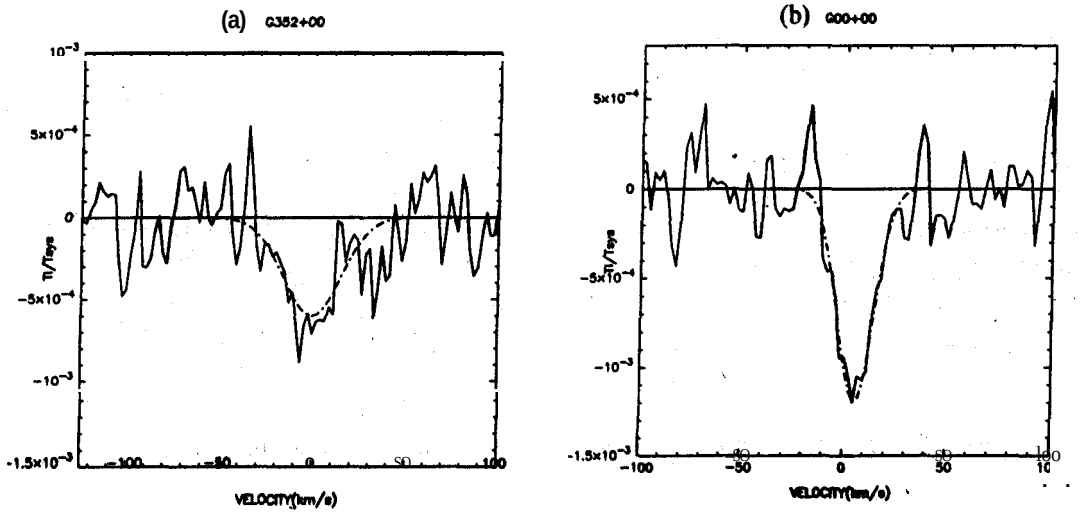

Figure 3.10 Spectra observed towards G352+00 and G00+00. The solid line is the observed spectrum and the dash-dotted line is the Gaussian fit to the absorption profile.

The Galactic Centre: A strong absorption line of carbon was detected from the direction of the Galactic centre as shown in Fig 3.10 (b). Carbon recombination lines have been observed from this direction in absorption at 75 MHz (EMA95) and 42 MHz (Smirnov *et. al.* al 1996). Emission lines at higher frequencies of 408 MHz (Pedlar *et. al.* 1978) and 328 MHz (Anantharamaiah 1985) have also been observed. The widths

of the lines observed at all the frequencies are very similar, unlike that towards Cas A. This suggests that tie pressure and radiation broadening effects are probably not important in this gas and the entire width is due to Doppler effects. Hence, we fitted a Gaussian-shaped function to characterize the observed profile. The dash-dotted line is the Gaussian fit to the observed profile (solid line). The fitted parameters are listed in Table 3.3. The peak line-to-continuum ratio in this line is of the order of 1×10^{-3} centred near 5 kms^{-1}. Modelling of the properties of the gas responsible for this spectral line is discussed in Chapter 5.

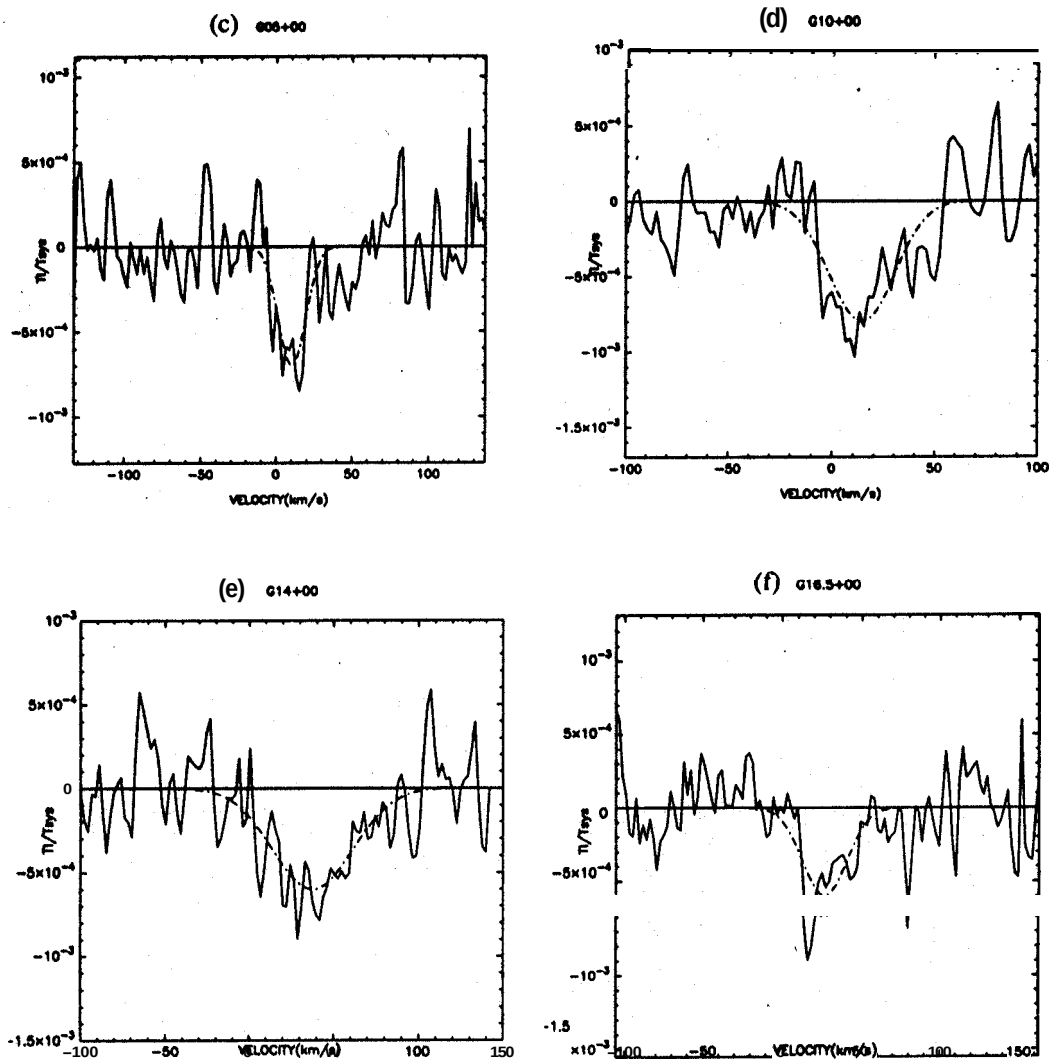

Figure 3.10 Spectra observed towards G05+00, G10+00, G14+00 and G16.5+00. The solid line is the observed spectrum and the dash-dotted line is the Gaussian fit to the profile.

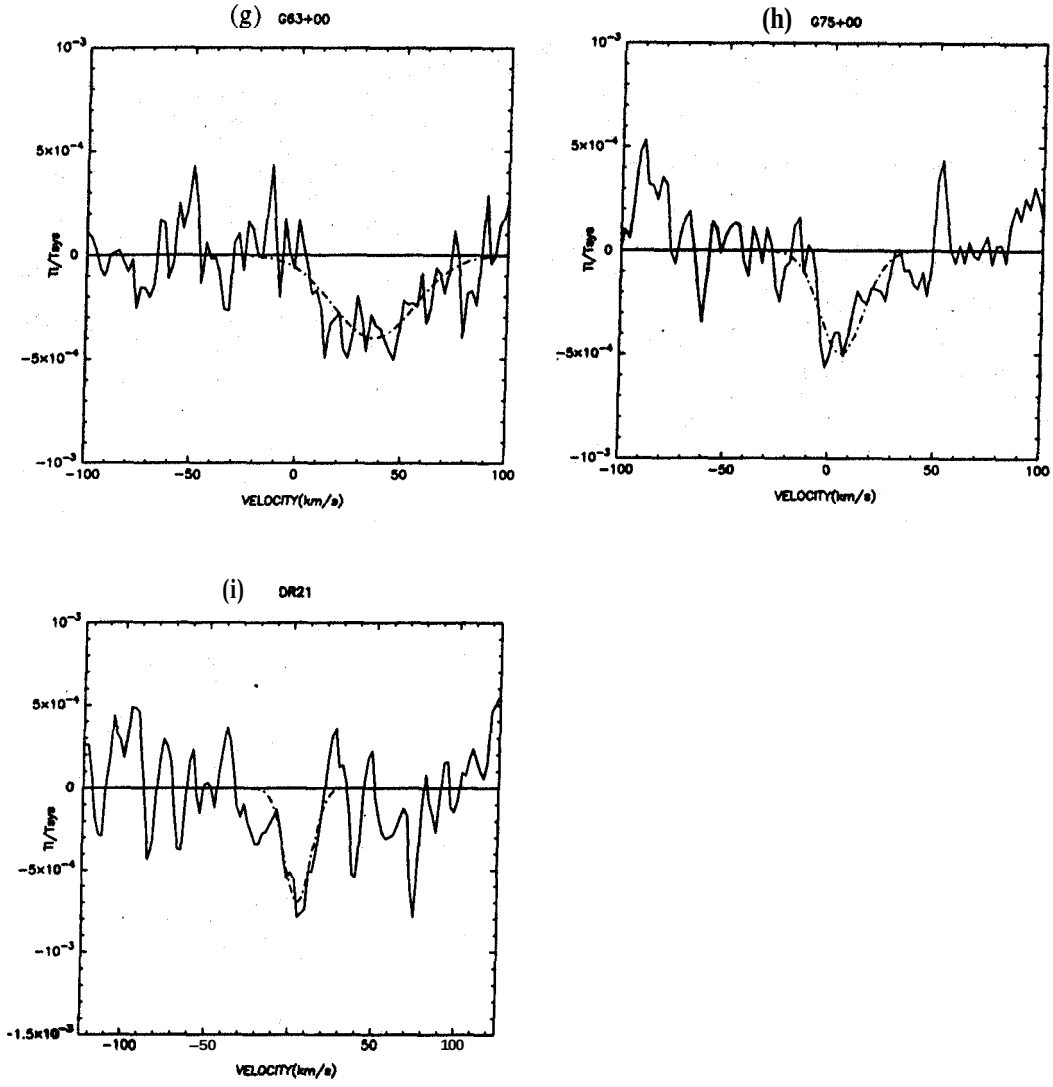

Figure 3.10 **Spectra observed towards G63+00, G75+00 and DR** 21. **The solid line is the observed spectrum and the dash-dotted line is the Gaussian fit to the profile.**

Positions in the Inner Galaxy: Carbon lines were detected in absorption **from all** the six observed directions in the inner galaxy (in the longitude range from **352°** to **17°).** This is similar to the result of **EMA95** who surveyed the inner **Galaxy** in carbon recombination lines near 76 **MHz** and detected lines **from** all their **pointings** within the longitude range **342°** to **20°.** We also detected carbon **lines from** DR 21, **G63+00** and G75+00. The spectra of all our detections towards directions in the inner Galaxy are shown in Fig 3.10. The line towards **G352+00** is at a negative radial velocity as expected from Galactic rotation. The lines detected towards all other directions are either at positive velocities or close to **0 kms^{-1}.** As mentioned earlier, the lines appear to be only Doppler-broadened and hence Gaussian profiles were used to characterise the observed

Table 3.3 **Parameters of the lines detected at 34.5 MHz with the Gauribidanur Telescope. The 1a errors on the fit parameters are given.**

No.	Source	34.5 MHz			
		T_l/T_{sys} 10^3	V_{lsr} kms^{-1}	ΔV_D kms^{-1}	$\frac{\int T_l d\nu}{s^{-1}}$
1	G352+0	−0.6f0.05	−0.8f1.5	36.4f.6	−2.6 ± 0.3
2	G00+00	−1.2 ± 0.1	5.2 ± 0.5	20.5 ± 1.2	−3.0 ± 0.5
3	G05+00	−0.7 ± 0.07	10.3 ± 1.0	21.0 ± 2.5	−1.8 ± 0.2
4	G10+00	−0.8 ± 0.06	14.4 ± 1.3	37.0 ± 3.2	−3.5 ± 0.4
4a	G10+00	−0.9 ± 0.07	9.4 ± 0.9	24.5 ± 2.0	−3.8 ± 0.3
		−0.5 ± 0.07	39.8 ± 1.4	18.9 ± 3.2	−3.8 ± 0.3
5	G14+00	−0.6 ± 0.04	37.7 ± 1.9	56.0 ± 4.5	−4.0 ± 0.4
6	G16.5+0	−0.6 ± 0.1	26.6 ± 1.4	32.6 ± 3.4	−2.3 ± 0.3
7	G63+00	−0.4 ± 0.04	36.4 ± 1.9	45.9 ± 4.4	−2.2 ± 0.2
8	G75+00	−0.5 ± 0.05	5.5 ± 1.2	24.4 ± 2.8	−1.5 ± 0.2
9	DR21	−0.7 ± 0.09	4.4 ± 1.1	18.5 ± 2.7	−1.6 ± 0.3

spectra. However, the lines seem to have widely varying widths ranging from about 18 kms^{-1} towards DR 21 to 56 kms^{-1} towards G14+00. It may be recalled that EMA95 observed linewidths (near 76 MHz) ranging from 5 kms^{-1} to 47 kms^{-1} in the inner Galaxy. The Gaussian fits (dash-dotted line) superposed on the observed spectra (solid line) are shown in Fig 3.10. Table 3.3 lists the line parameters obtained by fitting Gaussian functions to the observed profiles. The line-to-continuum ratios of these lines range from a few times 10^{-4} to 10^{-3} and the integral over the line width ranges from 1.5 to 4 s^{-1}.

The carbon line observed towards G10+00 seems to be composed of two components. We were able to obtain high signal-to-noise single and double component fits to this profile and the parameters are listed in Table 3.3. A similar trend is also seen in

the profiles towards G05+00 and the G14+00.

Relatively strong absorption lines towards DR 21 and G75+00 have been observed near 25 MHz by Golynkin & Konovalenko (1990) and Konovalenko (1984). We have also detected lines towards these two directions as shown in Fig 3.10.

Table 3.4 **Details of the Non-Detections at 34.5 MHz**

No.	Direction	T_{rms}/T_{sys} x 10^3 ($AV = 4.4$ kms^{-1})	Effective Integ hours	T_{rms}/T_{sys} x 10^3 ($AV = 20$ kms^{-1})
1	G342+00	0.35	63.5	0.12
2	G45.2+00	0.23	45.8	0.09
3	S140	0.39	24.3	0.07
4	W3	0.39	238.8	0.18
5	W51	0.20	69.0	0.09
6	G81+00	0.31	114.0	0.09
7	G100+00	0.20	178.3	0.11
8	G25+00	0.23	78.3	0.08
9	G55+00	0.23	50.7	0.10
10	G97+00	0.29	91.5	0.08
11	G99+00	0.33	169.5	0.22
12	G50+00	0.27	108.0	0.13
13	G85+00	0.34	41.7	0.09
14	W49	0.46	42.9	0.20
15	CYGLOOP	0.16	99.8	0.05
16	CYGNUS A	0.23	62.3	0.11
17	G125+00	0.37	88.8	0.30
18	G130+00	0.37	128.5	0.19
19	G145+00	0.37	100.0	0.19
20	ORION	0.54	19.7	0.22
21	G224.6-2.4	0.22	49.1	0.11
22	G203.1+2.1	0.50	12.0	0.16
23	ROSETTE	0.34	37.5	0.12

Non-detections: The 5σ upper limit on T_l/T_{sys} in the spectra towards positions which do not show the presence of a signal at 34.5 MHz is $\sim 5 \times 10^{-4}$. The rms noise and the effective integration time of these spectra are listed in Table 3.4. The spectra were smoothed to a spectral resolution corresponding to a typical line width (~ 20 kms^{-1}) and the spectra were examined for the presence of a spectral line. The rms noise levels

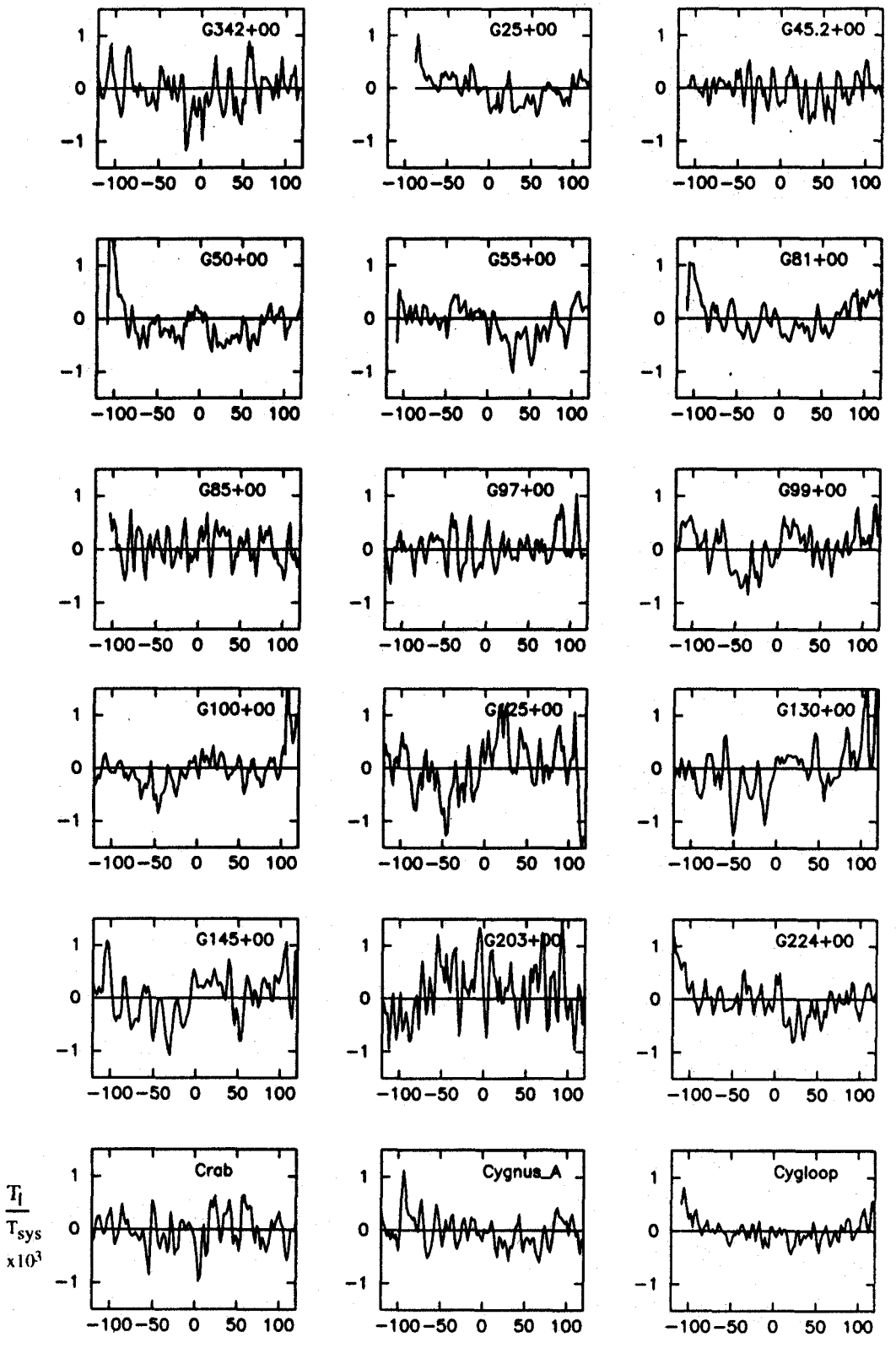

Figure 3.11 Non-detections at 34.5 MHz

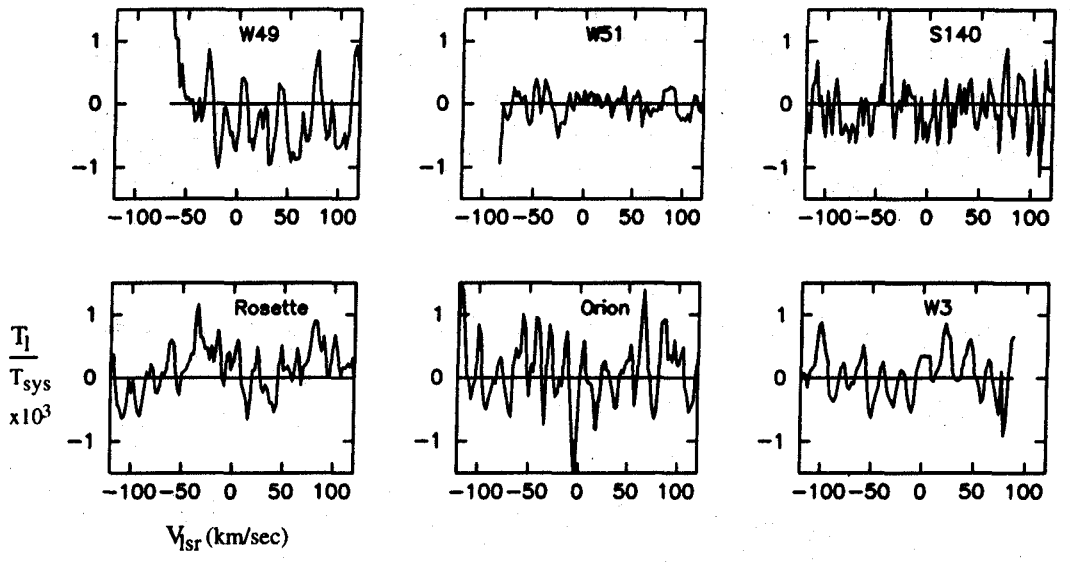

Figure 3.11 (contd) **Non-detections at** 34.5 **MHz**

after smoothing the spectra are also noted in **Table 3.4.** The observed spectra are shown in Fig **3.11.** The resolution of these spectra is 4.4 $\mathbf{kms^{-1}}$. In almost all the cases, only a linear baseline was subtracted from the data. Few of the spectra in the above figures seem to suggest the presence of a weak signal *e.g.* **G342+00, G55+00** and **G99+00.** However further observations are required to confirm these. In some of the cases, the spectrum is too noisy (like Orion, W49 etc) and in some cases, the spectra display a low-amplitude ripple (like **G99+00, G125+00** etc) which makes it difficult to determine the presence of signal in the spectra.

3.3 Observations with the Ooty Radio Telescope (ORT)

3.3.1 The Astrophysical Plan

Recombination lines of carbon which are observed in absorption at **34.5** MHz ($n \sim 575$) are expected to turnover into emission at **lower** n values due to inversion of level populations resulting in stimulated emission **(PAE89).** This turnover occurs because of the dominance of collisional processes in determining level populations at large quantum numbers and the dominance of radiative processes at lower quantum numbers. Collisions thermalize the large-n level populations, hence moving the excitation temperature closer to the kinetic temperature. The transitions between these levels are seen in absorption against the strong non-thermal radio background. At **lower-*n*** radiative

processes lead to non-LTE populations leading to negative values of the derivative of the departure coefficient, b_n *i.e.* β_n. The inverted populations result in stimulated emission. This was observed at frequencies above 200 MHz in the direction towards Cas A (PAE89). The frequency at which this turnover occurs depends on the physical conditions existing in the partially ionized gas and can therefore be used to investigate these regions. To search for the emission counterparts at a higher frequency, a subset of the directions in the Galactic plane observed at 34.5 MHz using the Gauribidanur telescope were observed using the ORT which operates at a centre frequency of 327 MHz. Carbon lines in emission were detected in all the directions observed with Galactic longitudes $< 17°$. The carbon line-forming regions from where the recombination lines at 328 MHz and 34.5 MHz arise can be modelled using the observed line-to-continuum ratios. This was the main aim of these observations. Furthermore, the design of ORT allows observations with more than one angular resolution in the N-S direction in the total power mode. Since the interpretation of the observed ratio of the line-to-continuum strengths from positions in the Galactic plane depends on the extent of the line-forming region we undertook observations with two extreme angular resolutions with the purpose of obtaining a preliminary idea of the sizes of the line-forming regions.

The carbon recombination line at 328 MHz detected towards Cas A is narrow ($AV < 5\ \mathrm{kms}^{-1}$) (PAE89) because it is essentially Doppler broadened. If carbon recombination lines from positions in the Galactic plane sample ionized carbon gas similar to that observed in the direction towards Cas A, then these lines should primarily be Doppler-broadened near n=272. Lines due to transitions between large quantum numbers (like $n \sim 575$) are expected to be pressure broadened. Therefore modelling the line widths at different quantum numbers could be used to place limits on the electron density in the line-forming region.

3.3.2 The Observations

The Antenna & the Receiver:

The ORT (Swarup *et. al.* 1971) is an off-axis parabolic cylindrical reflector which is 530 m long in the north-south (NS) direction and 30 m long along east-west (EW). The total power beam of the telescope is $2° \times 5.6' \sec\delta$. The telescope is located on a sloping hill whose inclination is equal to the latitude of the place, so that the long axis (NS) of the telescope is parallel to the earth's axis. The telescope thus has an equatorial mount. A source can be tracked for about nine hours by mechanically rotating the telescope about the long NS axis. A declination coverage of $\pm 35°$ is achieved through electrical

steering. Recently, the declination range of the telescope has been extended to $\pm 60°$. Although the geometrical delay is compensated, the sensitivity reduces steeply towards higher declinations because of projection effects and the primary beam of the individual dipoles at the feed.

The feed consisting of 1056 dipoles, mounted at the focus of the off-axis parabola are divided into 22 groups of 48 dipoles each. These groups are referred to as 11 north modules and 11 south modules. The signal collected by each of the 48 dipoles within each module is amplified and passed through a phase shifter. The signals are then combined in a Christmas-tree configuration to get the module output. The output of each module is mixed with a first local oscillator frequency near 296.5 MHz which includes the local standard of rest velocity corrections, to generate an IF at 30 MHz which is then brought to the receiver room. The delay and phase compensation for the 22 modules is provided at the IF stage using cables. The 30 MHz signal from the 22 modules are combined in 12 different phase combinations to obtain 12 simultaneous beams in the NS direction. The 12 beams span $\pm 18'$ and are separated by $3'\sec\delta$ in declination. The total power beam is $2° \times 5.6'\sec\delta$. In our observations, beam numbers 7 and 5 of these 12 were used. A provision to tap signal from any of the 22 modules is available. Hence, single-module observations with a resolution of $2' \times 2°\sec\delta$ are possible. The sensitivity of the ORT, when it is pointed within the declination range $[-35°, 35°]$, is ~ 2.6 K/Jy and the effective collecting area is ~ 7300 m^2. The sensitivity falls off at larger declinations. The system temperature of the ORT is about 150 K when pointed away from the Galactic plane.

An eight-line receiver specially developed for RRL observations with the ORT (Anish Roshi & Anantharamaiah 1997) was used for these observations. The total bandwidth of the ORT is 15 MHz centred at 326.5 MHz. This band contains four α transitions (*i.e.* $\Delta n = 1$) with the lower quantum number, $n = 270$, 271, 272, 273. The corresponding frequencies are 332.419, 328.759, 325.153, 321.599 MHz. Since observing these four transitions simultaneously would be equivalent to increasing the integration time by a factor of four, the eight-line receiver was designed to observe these four transitions simultaneously in any two beams out of the total 12 beams formed by the beam forming network. In this receiver (Anish Roshi & Anantharamaiah 1997), the 30-MHz first IF is further down-converted to 768-kHz basebands using a single-sideband system (SSB). Eight such systems are employed to realize the eight-line receiver. The LO frequencies for the SSB system are chosen so as to centre the basebands at the four recombination line frequencies. The basebands are split into two and one part is taken to the digital spectrometer, whereas the other half is connected to a total power detector.

As the spectrometer is a one-bit autocorrelator, the total power detector provides the amplitude calibration.

The baseband signals are sampled, digitized and correlated in a 512-channel, one-bit autocorrelator (Subrahmanyan 1989). A recirculator has been used to increase the number of correlator channels to 768 and to process all the eight bands simultaneously. The spectral resolution is 0.9 kms^{-1} (1 kHz).

A PC-based data acquisition system (DAS) records the correlation counts from the 768-channel correlator.

Observations

The observations with the ORT were carried out in two sessions: March-April 1995 and October 1995. Since the aim of these observations was to search for the emission counterpart of the carbon lines seen at 34.5 MHz, a subset of the positions observed at 34.5 MHz were observed with the ORT. In the first session, 13 positions were observed with the resolution of the entire telescope (*i*.e. 2° x 6') whereas in the second session, 10 positions with positive detections in the first round of observations were investigated with the resolution of a single module (*i.e.* 2° x 2°).

Pointing the telescope at a declination outside the ±35° range leads to reduced sensitivity. Inspite of this we observed Cas A ($6 \sim 59°$) which is a strong source with a flux density of ~ 6000 Jy near 328 MHz and we were successful in detecting lines near n=271.

The details of the sources observed, their coordinates, the effective integration times and the rms noise on the spectra are listed in Table 3.5.

Each source was tracked for at least 6 hours which was expected to give a theoretical noise of $\Delta T_{rms}/T_{sys} = 1.7 \times 10^{-4}$ if all the four lines were averaged. On the average, the noise in most of the full-telescope spectra was $\sim 2.0 \times 10^{-4}$. The noise in most of spectra obtained from the single-module observations was typically $\sim 1.5 \times 10^{-4}$ as listed in Table 3.5. The reference spectrum was measured by switching the first LO frequency every second by 375 kHz. This resulted in the line being shifted within the 768 kHz band and saving of telescope time.

A typical observing run began with a measurement of T_{sys} with respect to a reference position. In our observations, since beam 7 was pointed at the position of interest, beam 5 was directed to a position 6' south of beam 7. The line observations towards tlie selected direction were started after the calibration run. Reference spectra were measured by switching the frequency. The 'ON' and 'OFF' spectra were recorded by tlie DAS and the data reduced in the offline data analysis package.

Table 3.5 **Sources searched for Carbon Lines near 328 MHz**

No.	Source	α(1950) hh mm ss	δ(1950) ° ′ ″	Full Telescope $\frac{T_{rms}}{T_{sys}}$	Full Telescope t_{eff} hrs	Single Module $\frac{T_{rms}}{T_{sys}}$ 10^3	Single Module t_{eff} hrs
1	G355+00	17 29 54	-33 08 01	0.19	29.0	0.13	34.7
2	G00+00	17 42 27	-28 55 00	0.16	23.0	0.11	34.5
3	G05+00	17 54 00	-24 37 59	0.15	20.5	0.13	34.4
4	G10+00	18 04 47	-20 17 51	0.17	25.7	0.13	37.1
5	G14+00	18 12 59	-16 48 00	0.20	19.3	0.19	20.1
6	G16.5+00	18 17 57	-14 36 18	0.19	33.9	0.15	31.2
7	G30+00	18 43 29	-02 39 48	0.26	16.0	-	-
8	G50+00	19 21 02	15 02 41	-	-	0.17	28.2
9	G62+00	19 46 15	25 29 40	0.19	26.1	0.15	33.9
10	W49	190851	090227	0.20	20.7	0.17	42.9
11	W51	19 20 17	14 02 01	0.20	14.5	0.15	26.5
12	G75+00	20 19 02	36 26 46	0.20	30.7	-	-
13	NGC2024	05 39 11	-01 55 50	0.20	14.5	-	-
14	Cas A	23 21 11	58 33 48	0.15	25.0	-	-

Data Reduction

In the offline data reduction software, the one-bit data were Van Vleck corrected and the power spectra obtained (Weiner-Khinchin Theorem). Hanning smoothing of the observed spectra gave a spectral resolution of 2 kHz ($\sim$ 1.8 kms^{-1}). The difference ($\frac{ON-OFF}{OFF}$) spectra were visually inspected and those corrupted by interference were edited. Each spectral channel was assigned a weight which was updated when any channel showing interference was edited. At the end, all the edited spectra were averaged to obtain four final spectra corresponding to the four transitions., These spectra were then converted to the UniPOPS scans format. In UniPOPS, all the four transitions were folded in the frequency domain and averaged with appropriate channel weights to obtain the final spectrum towards any direction. The integration time for any spectrum was calculated from the channel weights.

3.3.3 The Results

Out of the total 14 positions (see Table 3.5) that were searched in carbon recombination lines at 328 MHz, lines were detected in emission from 8 of these directions with beam

7 and from 6 positions with beam 5 and a *single* module.

The spectra towards the positions of positive detections in the Beam 7 and Beam 5 (which are separated in the north-south by 6') are shown in Fig 3.12 and Fig 3.13 respectively. The line strengths observed with Beam 7 of the ORT are found to be systematically weaker than those with the adjacent beam, Beam 5. This is due to some instrumental problem. Since Beam 5 is only 6' away from Beam 7 and hence still looking at the Galactic plane, these high signal-to-noise ratio spectra are used for further analysis. Fig 3.14 shows the spectra obtained with a single module of the ORT.

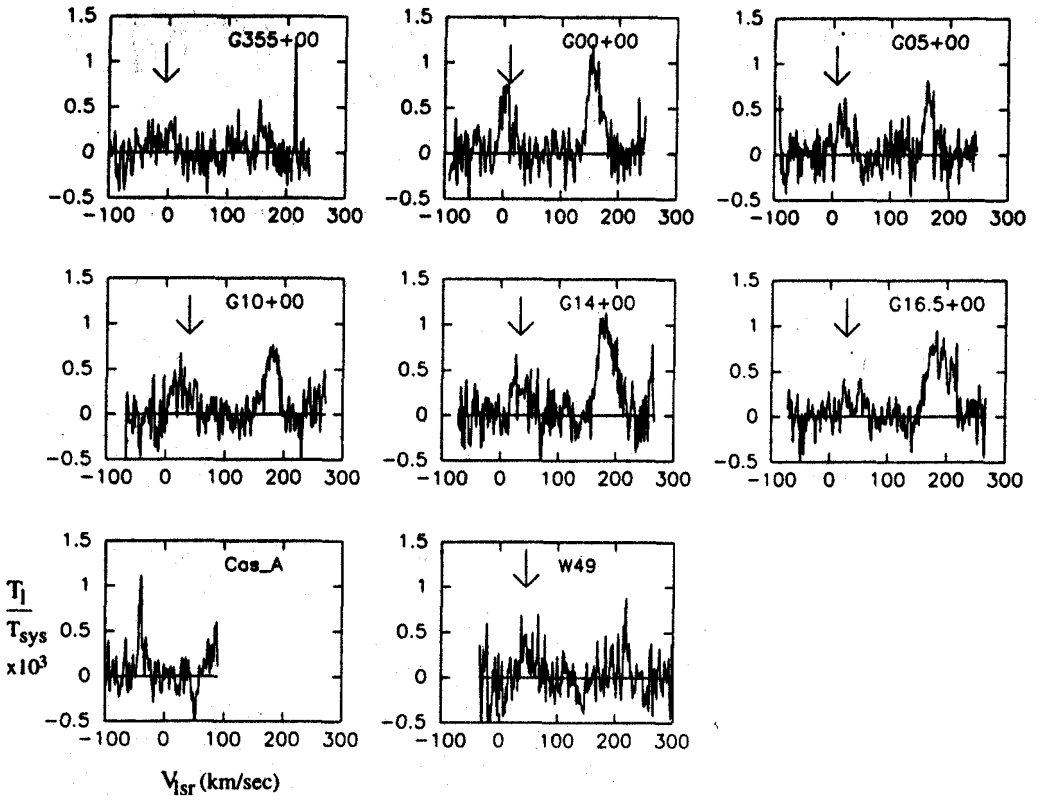

Figure 3.12 **Spectra of Lines detected at 328 MHz with Beam 7 of the ORT. The arrow indicates the carbon line. The stronger line is of hydrogen. The angular resolution is 2° x** 6'.

Hydrogen recombination lines at 328 MHz were detected in 11 of the 14 directions that were observed. These are relatively strong lines appearing near radial velocities of 150 kms^{-1} in the Figs showing the line spectra. The velocity scale in the spectra is with respect to the carbon line. No hydrogen lines were detected towards Cas A, NGC2024 and G62+00 to the limits listed in Table 3.5. Hydrogen recombination lines at 328 MHz have been detected from all observed positions in the Galactic plane with $l < 40°$

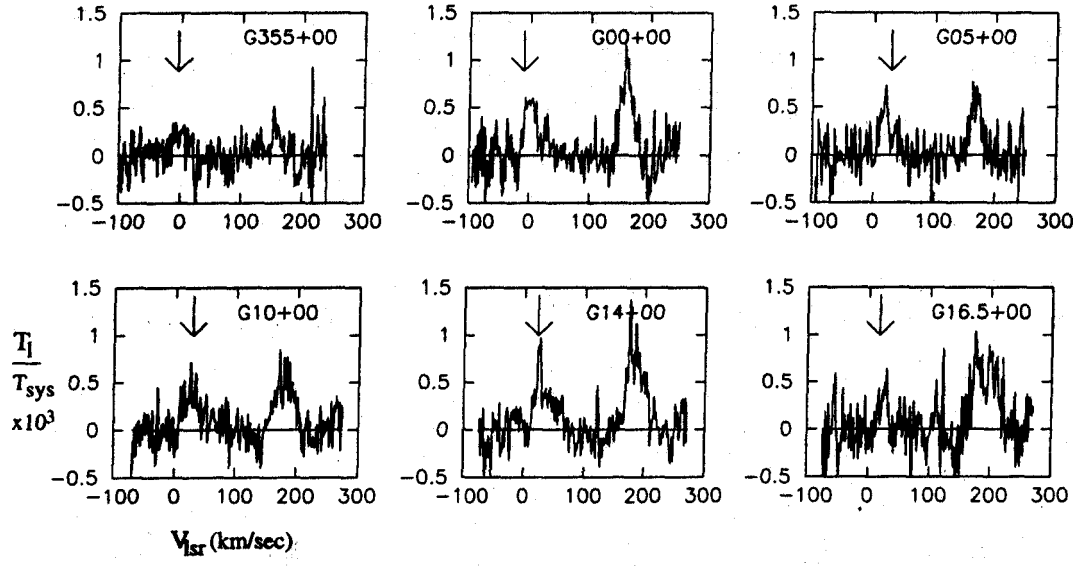

Figure 3.13 Spectra of Lines detected at **328 MHz** with Beam **5** of the ORT. The arrow indicates the carbon line. The stronger emission is the hydrogen line. The angular resolution is 2° x 6.

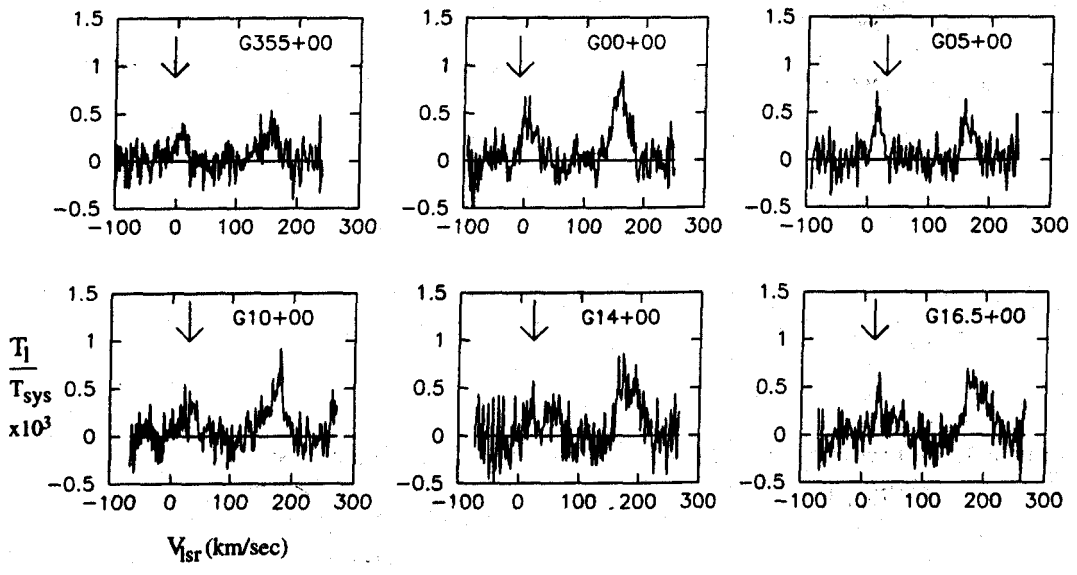

Figure 3.14 Spectra of Lines detected at **328 MHz** with a Single Module of the ORT. The arrow indicates the carbon recombination line. The other more stronger emission line is of hydrogen. The angular resolution is 2° x 2°.

Table 3.6 **Parameters of the Carbon lines observed with the ORT. The numbers in the bracket are the** 1o **errors.**

No.	Source	C271α near 328 MHz											
		ORT Beam 7 2° × 6′				ORT Beam 5 2° × 6′				Single Module 2° × 2°			
		T_l/T_{sys} 10^3	V_{lsr} kms^{-1}	ΔV_D kms^{-1}	$\frac{\int T_l d\nu}{s T_{sys}}$	T_l/T_{sys} 10^3	V_{lsr} kms^{-1}	ΔV_D kms^{-1}	$\frac{\int T_l d\nu}{s T_{sys}}$	T_l/T_{sys} 10^3	V_{lsr} kms^{-1}	ΔV_D kms^{-1}	$\frac{\int T_l d\nu}{s T_{sys}}$
1	G355+0	0.2	-17.6	45.0	10.5	0.2	-8.8	21.9	5.1	0.3	0.8	20.1	6.9
		(0.02)	(3.0)	(7.1)	(2.5)	(0.04)	(1.9)	(4.4)	(2.5)	(0.02)	(0.7)	(1.7)	(0.7)
2	G00+00	0.65	-3.4	18.7	14.2	0.61	-4.1	20.6	14.8	0.43	0.5	27.0	13.5
		(0.07)	(0.5)	(1.1)	(2.6)	(0.07)	(0.5)	(1.1)	(1.8)	(0.05)	(0.6)	(1.5)	(1.8)
3	G05+00	0.4	10.7	24.2	11.1	0.5	12.3	19.0	10.9	0.52	8.2	16.2	9.8
		(0.03)	(0.8)	(1.9)	(1.0)	(0.03)	(0.6)	(1.4)	(0.9)	(0.02)	(0.4)	(0.9)	(0.6)
4	G10+00	0.3	20.1	32.8	11.1	0.4	20.3	29.9	13.7	0.26	21.7	36.3	10.7
		(0.02)	(1.3)	(3.0)	(1.2)	(0.02)	(0.8)	(2.0)	(1.1)	(0.02)	(1.2)	(2.9)	(1.0)
5	G14+00	0.3	27.7	31.9	10.9	0.5	24.6	32.7	18.8	0.2	36.5	54.6	12.7
		(0.02)	(1.0)	(2.3)	(0.9)	(0.06)	(1.7)	(3.9)	(1.2)	(0.04)	(3.7)	(8.7)	(4.1)
6	G16.5+0	0.2	32.7	39.1	9.1	0.45	20.3	11.4	6.5	0.48	20.0	12.7	7.0
		(0.02)	(2.3)	(5.3)	(2.3)	(0.1)	(1.4)	(3.3)	(0.8)	(0.07)	(0.8)	(2.0)	(0.6)
7	G30+00	< 0.15	-	6.2	< 1.1	< 0.20	-	6.2	< 1.5	x	x	x	x
8	W49	0.3	42.2	30.7	10.7	< 0.17	-	6.2	< 1.2	< 0.10	-	6.2	< 1.0
		(0.06)	(1.5)	(3.6)	(2.4)	-	-	-	-	-	-	-	-
9	W51	< 0.12	-	6.2	< 1.1	< 0.14		6.2	< 1.2	-	-	-	-
10	G50+00	x	x	x	x	x	x	x	x	0.2	50.5	35.4	8.3
										(0.02)	(1.9)	(4.6)	(2.5)
11	G62+00	< 0.14	-	6.2	< 1.2	< 0.13	-	6.2	< 1.1	<0.42	-	8.0	<3.7
12	G75+00	< 0.12	-	6.2	< 1.1	< 0.19	-	6.2	< 1.4	x	x	x	x
13	Cas A	1.2	-47.5	5.0	7.0	x	x	x	x	x	x	x	x
		(0.1)	0	(0.5)	(0.5)	x	x	x	x	x	x	x	x
14	NGC2024	< 0.11	-	6.2	< 1.1	< 0.11	-	6.2	< 1.1	x	x	x	x

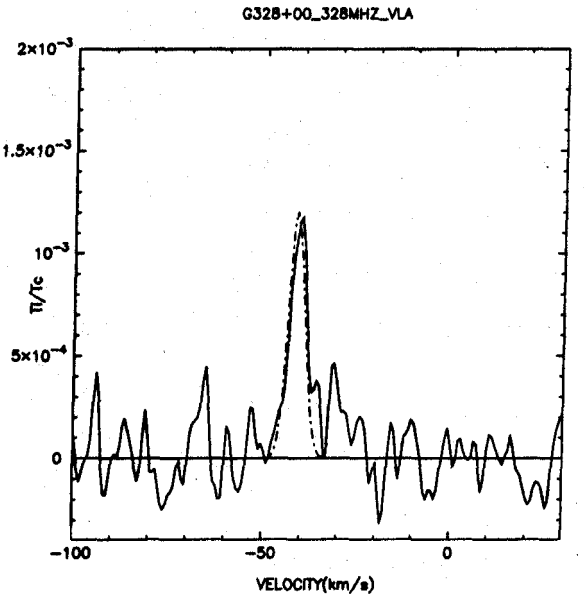

Figure 3.15 C270α spectrum observed towards Cas A. The solid line shows the observed spectrum while the dash-dotted line shows the Gaussian fit to the profile with a peak line-to-continuum ratio of 1.2 $\times$ 10^{-3}, radial velocity of –47.5 kms^{-1} and a width of 5 kms^{-1}.

(Anantharamaiah, 1985). These lines are believed to originate in the low-density, hot gas associated with normal HII regions. As the work in this thesis is concerned only with interpretation of carbon recombination lines at low frequencies, hydrogen lines are not discussed here.

A narrow (AV $\sim$ 5 kms^{-1}) carbon line was detected towards Cas A. This direction has been extensively studied in carbon recombination lines over a wide range of quantum numbers (references in PAE94) and also in HI 21-cm line (Bieging *et.al.* 1991) and several molecular lines (references in Anantharamaiah *et.al.* 1994). High-frequency recombination lines have been shown to be only a few kms^{-1} wide as also seen in the present detection. The observed profile with a Gaussian-shaped function superposed on it is shown in Fig 3.15. Although two components in the Perseus arm corresponding to velocities of -47 kms^{-1} and -39 kms^{-1} have been observed at this frequency in other observations, we observe only a single component at a velocity of -47.5 kms^{-1} probably due to the poor signal-to-noise ratio of the spectrum. The weak Orion arm component observed at -1.6 kms^{-1} (Anantharamaiah *et.al.* 1994) is not seen in our spectrum. If the physical properties of the carbon line-forming regions in the Galactic plane are similar to

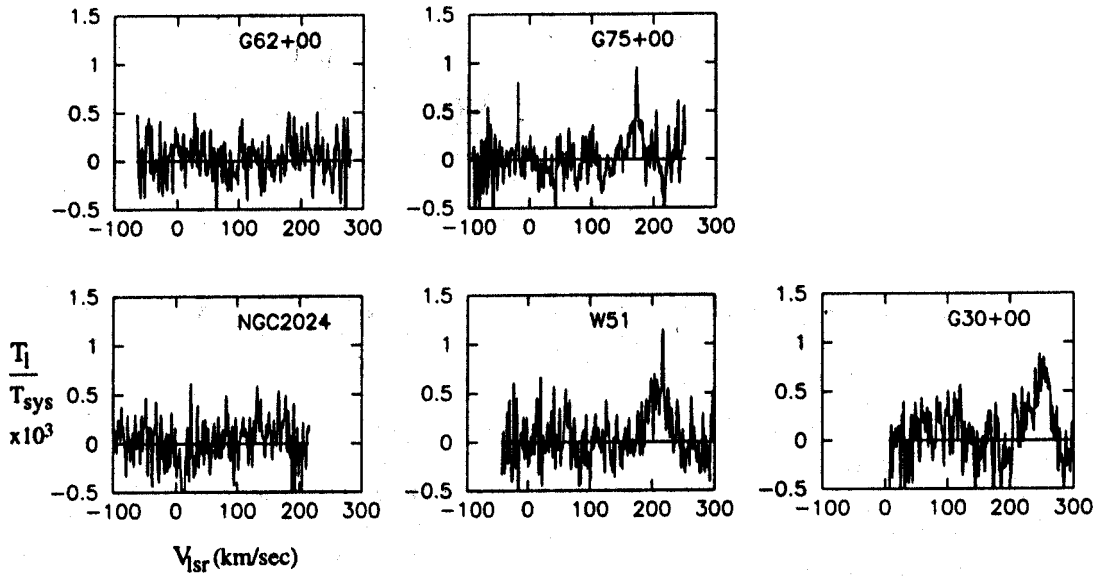

Figure 3.16 ORT Beam 7 Non-Detections

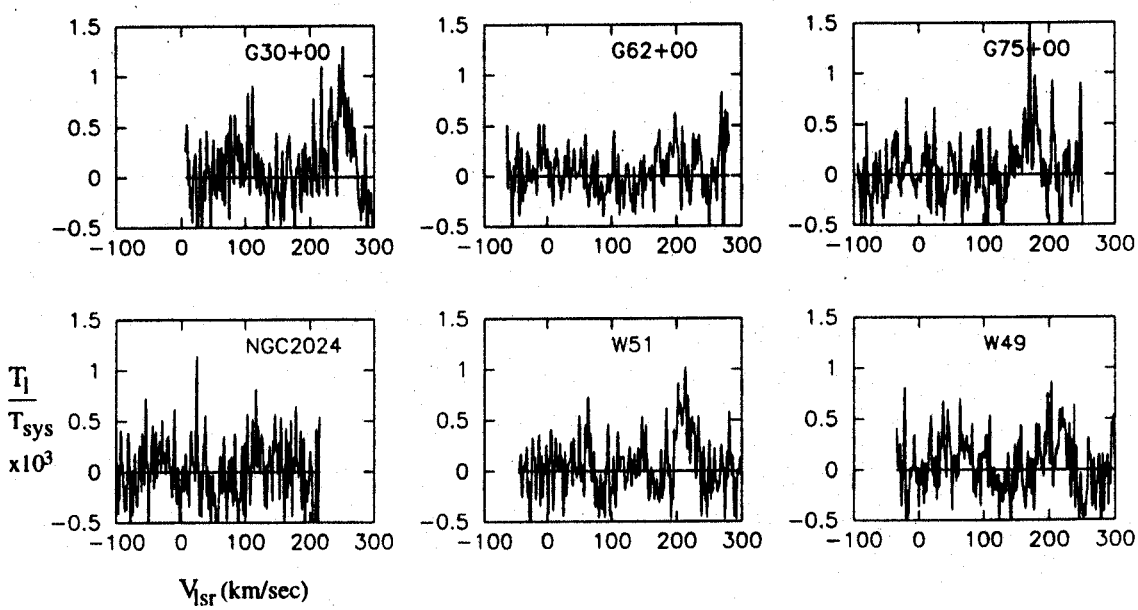

Figure 3.17 ORT Beam 5 Non-Detections

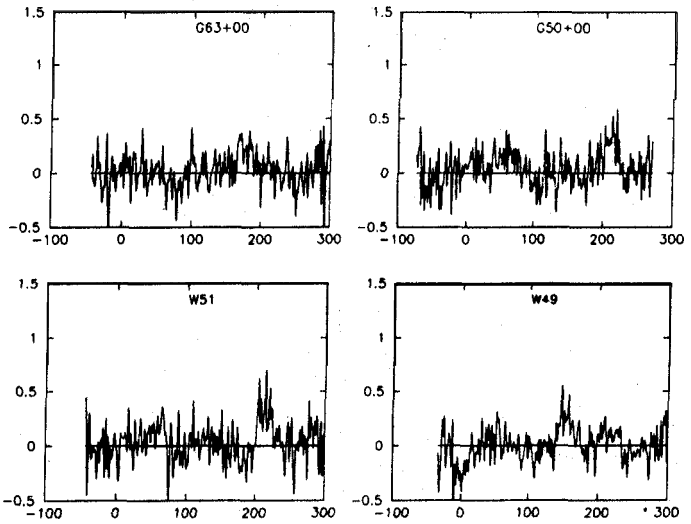

Figure 3.18 ORT Single Module Non-Detections

the gas along the line-of-sight towards Cas A, then the lines due to transitions between quantum numbers near n=272 are expected to be essentially Doppler-broadened. The carbon line profiles were hence fitted with Gaussian-shaped functions. In Table 3.6, results of the Gaussian fits to the lines detected in the adjacent beams (beams 7 and 5) of the ORT and using a single module are listed. The carbon lines detected from directions other than Cas A were broad ($\Delta V \geq 20$ kms^{-1}) and comparatively weak. The effective integration time on each of the direction observed was on the average more than 25 hours and the $\Delta T_{rms}/T_{sys} \sim 2 \times 10^{-4}$ in most of the spectra. Most of the positions that were seen in carbon lines with the full telescope resolution were also detected in the single-module observations with comparable strengths, suggesting that the carbon line region may be of the order of or larger than 2° in angular extent.

The spectra towards the positions which failed to show a carbon recombination line are shown in Fig 3.16, 3.17 and 3.18. The 1σ limit on the carbon line are listed in Table 3.5. The negative spike-like feature observed in the spectrum towards NGC2024 shown in Fig 3.16 is due to interference in the OFF spectrum which appears as a negative feature in the difference spectrum. The spike observed in the spectrum of G75+00 in the same figure also seems to be characteristic of a weak interference spike which escaped notice during data editing. It is possible that it is a feature arising due to the ISM, but further observations are needed to confirm this. As it is an ambiguous signal, we do not treat it as a real feature.

All the positions in the inner galaxy ($l < 20°$) that were observed with the Gauribidanur and Ooty radio telescopes have yielded a positive detection, inspite of the very different angular resolutions of the two observations. The angular resolution at 34.5 MHz was 21' x 25° whereas at 328 MHz, the coarsest resolution was 2° x 2'. The size of the ionized carbon region which gives rise to these lines is not known and the above result suggests that it may be large. If the cloud was much smaller than the beam at 34.5 MHz, then beam dilution would have probably made it unobservable. However, the peak optical depths and line widths observed at the two frequencies are comparable. These results are further discussed in Chapter 5.

3.4 Observations with the Very Large Array (VLA)

We used the VLA to image the recombination line emission towards Cas A and towards the position, G14+00. The details of these two observations are given separately in each of the following subsections.

3.4.1 The Astrophysical Plan

The aim of observing Cas A with the VLA was to establish the site of origin of the low-frequency carbon recombination lines arising in the gas in the Perseus arm by comparing its spatial distribution with that of the neutral components (H I & H_2) of the ISM.

The physical models for the ionized gas in front of Cas A (cold gas model with $T_e \sim 20$ K, $n_e \sim 0.3$ cm^{-3} and warm gas model with $T_e \sim 50$ K, $n_e \sim 0.1$ cm^{-3}) that have been fairly successful in explaining the observed optical depths of the carbon recombination lines suggest that the carbon lines arise in either molecular or atomic gas. Recently, PAE94 have analysed the carbon recombination line data towards Cas A and showed that the carbon line observations can be explained only if the carbon lines originated in the atomic hydrogen gas. Comparison of the distribution of ionized gas across Cas A with that of the neutral gas would be useful in providing additional evidence for the above conclusion. The carbon RRL and the lines from neutral gas are found at similar velocities suggesting that they arise in either coexistent or nearby clouds. High-angular resolution images of Cas A have been made in the H I 21-cm line arid in many molecular lines like OH, H_2CO, ^{12}CO and these have revealed different morphologies for the atomic and molecular gas in the Perseus arm towards Cas A. If Cas A can be imaged at comparable resolutions in a recombination line, then additional knowledge on the site of origin of these lines can be obtained. Since PAE89 have shown

that carbon recombination lines are detectable at 325 MHz, we used the VLA to image Cas A in C270α with a resolution $\sim$ 25" and compare its spatial distribution with those of atomic and molecular gas. The results obtained by Anantharamaiah *et.al.* , (1994) with a low-angular resolution of 2.5' for C270α favoured the atomic gas as the site of origin of the carbon recombination lines.

Table 3.7 VLA observations of G14+00 and Cas A

No.	Parameter	Source	
		G14+00	Cas A
1	Field Centre: $\alpha(1950)$	$18^h12^m59^s$	$23^h21^m10^s$
	$\delta(1950)$	$-16°48'03''$	58'32'29'
2	Observing Sessions	June 1995	December 1991
3	Telescope Time	4.5 hours	10 hours
4	Observed Transitions	270α, 271α	C270α
5	Rest Frequencies (Carbon)	332.419 MHz	332.419 MHz
	328.76 MHz		
6	Observing Band	P-baud (90cm)	P-band (90cm)
7	Primary Beam	150'	150'
8	VLA antenna configuration	D	B
9	Shortestspacing	0.035 km	0.21 km
10	Longest spacing	1.03 km	11.4 km
11	Observing Mode	41F	2AC
12	Expected T_{sys}	> 650K	> 750K
13	Total bandwidth	781 kHz	98 kHz
	(693 kms^{-1})	(88 kms^{-1})	
14	Number of Channels	64	128
15	Frequency Resolution	12.207 kHz	1.526 kHz
16	Velocity Resolution	11 kms^{-1}	1.38 kms^{-1}
17	Amplitude Calibrator	3C286	3648
18	Phase Calibrator	1827-360	2348+643
19	Bandpass Calibrator	1827-360	Cygnus A
20	Synthesized beam	321.4" x209"	27" x21"
	(natural weighting)		
21	Rms noise, line	25 mJy/beam	35 mJy/beam
22	Rms noise, continuum	150 mJy/beam	375 mJy/beam

The main aim in observing G14+00 with the VLA was to determine the typical angular extent of a recombination line-forming cloud in the Galactic plane which is crucial in the interpretation of the observed lines. Unlike the case of Cas A where the

angular extent of the strong, non-thermal continuum source determines the cloud size sampled by all observations, the extent of the cloud towards positions in the Galactic plane which are free of strong, discrete radio sources is unknown. Till date, the low frequency lines of carbon and hydrogen have only been observed using large, single-aperture telescopes. Carbon lines near 325 MHz have been detected in emission from 12 positions in the Galactic plane using the ORT (Anantharamaiah 1986) with an angular resolution of 2' x 6' and lines near 76 MHz have been detected in absorption using the Parkes radio telescope with an angular resolution of 4' (EMA95). Hydrogen recombination lines near 325 MHz (H272α) have been detected from almost every position in the Galactic plane ($-20° < l < 75°$) using the ORT (Anantharamaiah 1985, Anish Roshi & Anantharamaiah 1997). Due to the low-angular resolution of these observations, the interpretation of the observed lines are subject to many uncertainties, principally due to the unknown angular size of the emitting or absorbing regions. High-resolution, high-sensitivity observation of these regions in recombination lines near 330 MHz using the VLA is ideal in gaining useful insight into the angular distribution of these regions. We selected the position G14+00 for observing with the VLA. Both hydrogen and carbon lines near 325 MHz have been detected towards this direction using the ORT (Anantharamaiah 1985) with a resolution of 2° x 6'. The carbon line detected from this position is the strongest (peak line strength $\sim$ 160 mJy) amongst the 12 directions towards which lines were detected with the ORT and hence it was chosen for further investigation. The detectability with the VLA depends critically on the spatial structure of the line-emitting region. If the lines arise in extended regions (almost filling the single-dish beam), then the emission will be resolved out by the VLA. But if the emission is patchy, then the VLA would be able to pick up line strengths of a few tens of mJy/beam. Either way, this observation would give useful information on the angular dimensions of the low-density, line-emitting region towards the position G14+00.

In Fig 3.19, the full ORT beam is traced on the 5 GHz continuum map (Altenhoff *et.al.* 1979) near the position G14+00. The VLA primary beam is also shown in the figure. It covers a wider region than that sampled by the full ORT beam and hence line emission from regions outside the ORT beam can also be studied.

3.4.2 Observations & Results

The details of the observations of Cas A arid G14+00 with the VLA are summarized in Table 3.7.

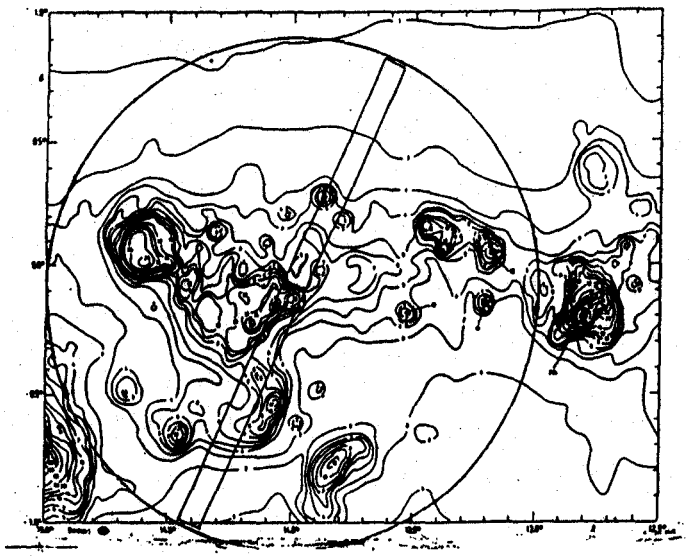

Figure **3.19 Galactic Plane near G14+00 at 5 GHz. The Ooty beam (rectangle) and a circle of 2° diametre which can be imaged with the VLA are indicated in the figure.**

G14+00: G14+00 was observed in one session in June **1995** for about **4.5** hours in the **D-configuration** of the VLA. The observing session began with a run on the primary calibrator (1328+307). G14+00 was then observed in **separate** scans each of **30** minutes. These scans were interspersed by observations of the phase and **bandpass** calibrator, **1827-360.** Since the carbon and hydrogen recombination lines are separated by **150 kms^{-1}** and the lines from G14+00 are expected to appear at a radial velocity close to **25 kms^{-1}**, the central velocity in the band was set to **−50 kms^{-1}** so that both the lines could be simultaneously observed in the band. The four-IF mode of the **correlator** which consisted of two circular polarisations (Stokes RR and Stokes LL) and two IF frequencies, was used. Two consecutive transitions (270α & 271α) were observed simultaneously.

The UV data **were** processed using the Astronomical Image Processing System (AIPS) developed by NRAO. The visibilities in the central three-quarters of the band were averaged to obtain the continuum (known in AIPS as **"Ch 0"**) data base. These visibility data were edited and calibrated using the phase and amplitude calibrators listed in Table **3.7.** The "dirty" image obtained by Fourier **transforming** the calibrated visibilities **was** deconvolved using the "CLEAN" algorithm which is implemented in the routine MX in AIPS. Natural weighting of the data gave a beam size of **321"** x **209" (5.4' x 3.5')** with PA = 1.5°.

A source which was free of spectral lines was chosen as the **bandpass** calibrator.

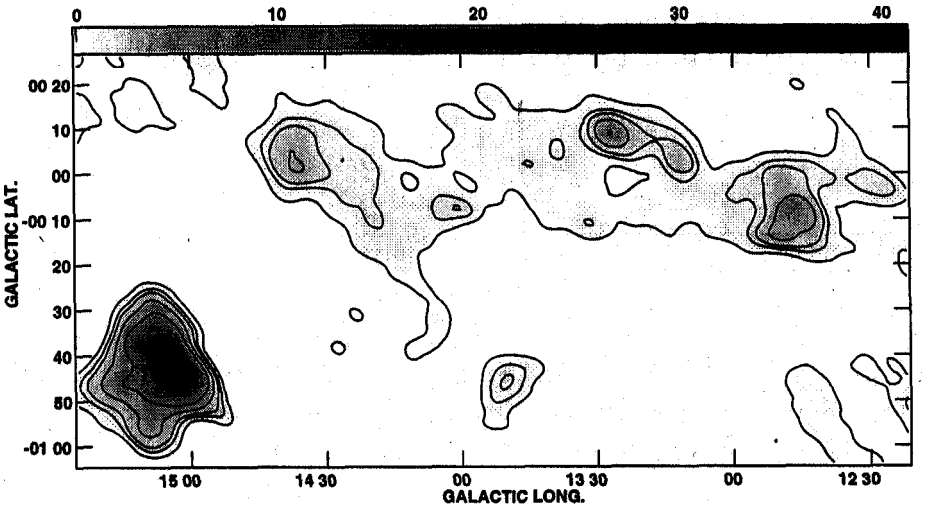

Figure 3.20 **Continuum Image of G14+00 at 330 MHz in Galactic coordinates. The contour levels are 1,3,5,10,20,50,100,110 in units of 0.4 Jy/beam and the grey scale flux range in the image ranges from 0 to 41 Jy/beam.**

Bandpasses were generated for all the antennas (using the task BPASS in AIPS) and were then applied to the source data. The continuum emission was subtracted from the line visibilities using the task **UVLIN** in AIPS which removed from all the visibilities, a linear baseline determined from channels which have no line emission. A line cube was obtained by Fourier transforming the residual visibilities using the task HORUS in AIPS. To obtain the maximum signal-to-noise ratio, natural weighting was applied to the visibilities.

Although we aimed at achieving an rms noise of 7-8 **mJy/beam** in the line images, severe problems due to interference forced us to discard more than 50 % of the visibilities. The rms noise on the line images that we ultimately obtained was 25 **mJy/beam.**

The continuum image of the **2°** field centred on **G14+00** at 330 MHz is shown in Fig 3.20. The rms noise on the continuum image is 150 **mJy/beam.** M17 (the bright source at the bottom-left corner of image) is the brightest source in the **2°** field with a peak brightness of 40 **Jy/beam.** This is a classical **HII** region **whose** central region is expected to become optically thick at low frequencies. For an optically thick nebula, the observed brightness temperature is a direct measure of its electron temperature as discussed in Chapter 2. We calculate a brightness temperature of 7885 **°K** for M17 using

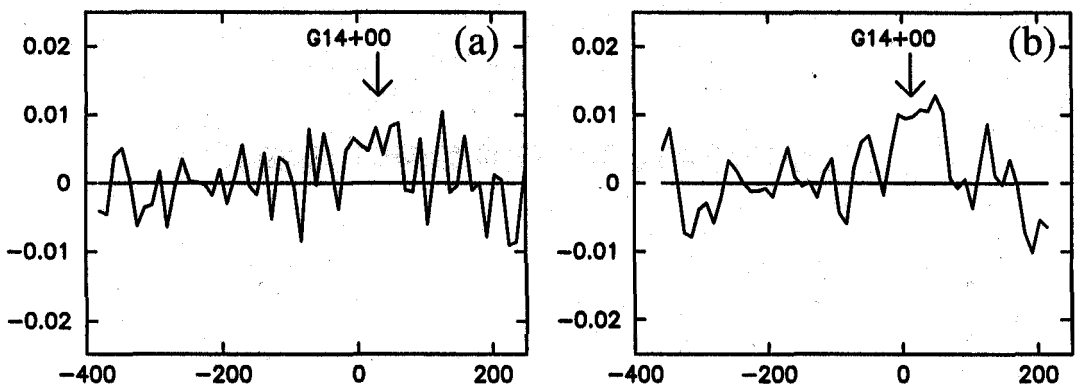

Figure 3.21 **Line emission integrated over some region near G14+00 which shows continuum emission (excluding M17):** (a) **The spectrum of the line emission over the entire continuum source near G14+00,** (b) **The spectrum shown in** (a) **has been hanning smoothed and a linear baseline has been removed to obtain this spectrum. The arrow indicates the probable hydrogen line.**

the peak brightness. This estimate agrees with the value calculated by Subrahmanyan & Goss (1996) using the peak brightness in M17 at 330 MHz with 1' resolution. The good agreement between the temperature calculated with a 5' beam and that calculated with a 1' beam suggests that the centre of M17 is optically thick over a 5' region. Other sources which are the low-frequency counterpart of the sources seen at 5 GHz (Altenhoff *et.al.* 1979) and 2.7 GHz (Reich *et.al.* 1990) can be identified in the field (Fig 3.20). Seven compact sources and a low-brightness envelope enclosing six of these sources is clearly seen in this figure.

The line images showed no detectable emission. Hence we do not show the images here. The rms noise on the line images is 25 mJy/beam (beam = 5.4' x 3.5').

The line emission was integrated over the envelope seen in continuum emission (Fig 3.20) and then divided by the continuum brightness (182 Jy) integrated over the same region to obtain the spectrum shown in Fig 3.21(a). The same spectrum is shown in Fig 3.21(b) after removing a linear baseline and applying further hanning smoothing. The position of the hydrogen line is marked by an arrow in the spectrum. It seems to show the presence of a hydrogen recombination line at a velocity of 25 kms^{-1}. No feature is visible where the carbon line is expected (*i.e.* at -150 kms^{-1} with respect to the hydrogen line). The rms noise on the spectrum shown in Fig 3.21(b) is 3 x 10^{-3}. A Gaussian of amplitude 1.2(0.13) x 10^{-2}, radial velocity, 25(5) kms^{-1}, and full-width at half maximum of 70(11) kms^{-1} fitted the observed profile well. The hydrogen line observed with the ORT (beam of 2° x 6') had a line-to continuum ratio of 1.4 x 10^{-3}(0.001), a radial velocity of 24.1(1.5) and a width of 38 kms^{-1} (Anantharamaiah

1985). The radial velocities of the lines from the two observations match well. However, the line-to-continuum ratio and the line widths detected in the present observation are larger than thoss detected by the ORT. One possible reason is that the ORT was sensitive to only a fraction of the continuum source (as depicted in Fig 3.22(b)). Moreover, the ORT beam extends well beyond the Galactic plane where no continuum emission is observed in Fig 3.22(b) and beam dilution effects may be responsible for the decreased line strengths.

In Fig 3.22(a), the line emission divided by the continuum (19 Jy), integrated over the continuum source within the ORT beam (Fig 3.22(b)) has been shown. The upper limit on the line-to-continuum ratio of carbon and hydrogen emission lines is 7.8 x 10^{-3} (3σ limit). This is consistent with the ORT results in which both the lines are of the order of 1 x 10^{-3}, way below our detection limit in these observatidns.

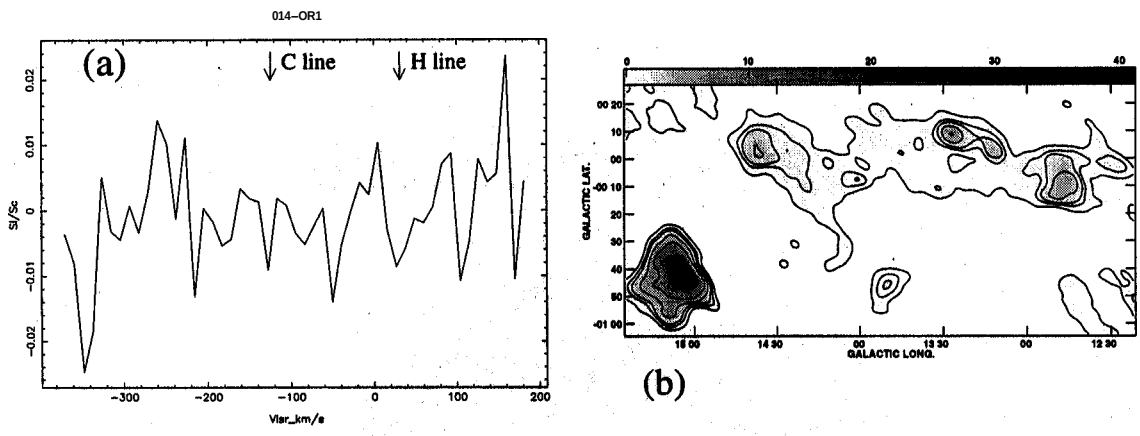

Figure 3.22 (a) **Spectrum showing the line emission over the common region of the full ORT beam and the continuum emission near G14+00 at** 330 **MHz.** (b) **The full ORT beam has been superposed on the** 330 **MHz continuum map of G14+00 obtained with the VLA.**

Cas A: Cas A was observed in four sessions during December 1991 in the B-configuration of the VLA for a total telescope time of 10 hours. The C270α ($\nu = 332.419$ MHz) line emission across Cas A was imaged. The programme source was observed for 35 minutes at a stretch. Observations of 2348+643 were interspersed to calibrate the phase. The primary and bandpass calibrators were observed once during each session.

AIPS was used to process the UV visibilities. The "Ch 0" image was generated using the procedure similar to that used for G14+00. Since, bandpass calibration involves dividing the source spectrum with the bandpass of the calibrator for each antenna, it is essential to choose a calibrator whose signal-to-noise ratio is comparable to or more than that of the programme source. Cas A (6000 Jy) is one of the strongest radio

continuum sources in the sky and hence Cygnus A (also close to 6000 Jy at 336 MHz) was chosen as the bandpass calibrator. Since Cygnus A has spatial structure which begins to get resolved on the longer baselines, the signal-to-noise ratio of the antenna bandpasses were not uniform. However, experimenting with an unresolved weaker source as the bandpass calibrator we found that the results obtained with Cygnus A were better than those with the weaker source and hence we used Cygnus A as the bandpass calibrator. The line data were calibrated for amplitude, phase and bandpass using standard procedures. As in the case of G14+00, the continuum emission was subtracted from the visibilities using the task UVLIN and HORUS was used to image the residual line visibilities after applying natural weighting. The images where line emission was detected were deconvolved using CLEAN. Spectra and maps of Cas A in C270α were obtained.

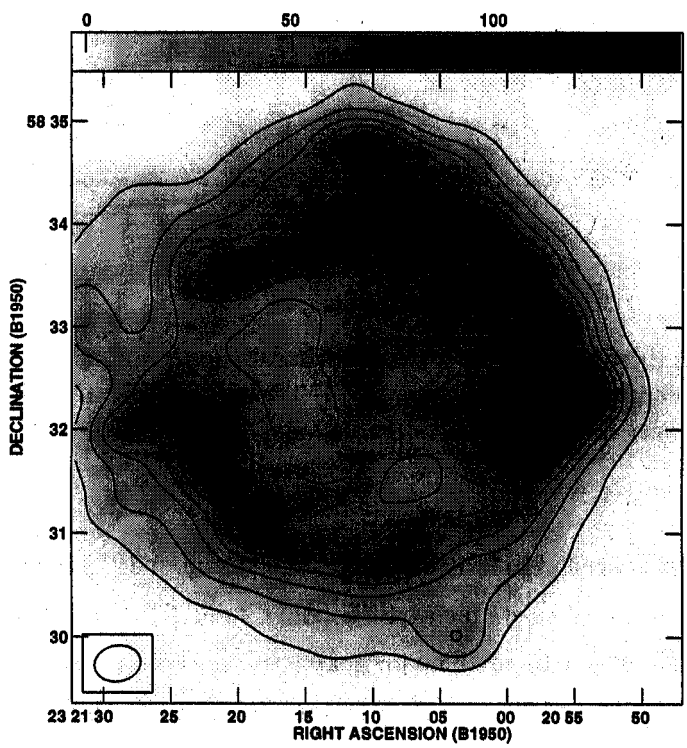

Figure 3.23 **Continuum Image of Cas A at 330 MHz - resolution: 26.9" × 20.9". The contour levels are 1,3,5,7,9,11,13,15,17,19,20 in steps of 7.2 Jy/beam. The grey scale flux range in the image is -2.4 to 144 Jy/beam.**

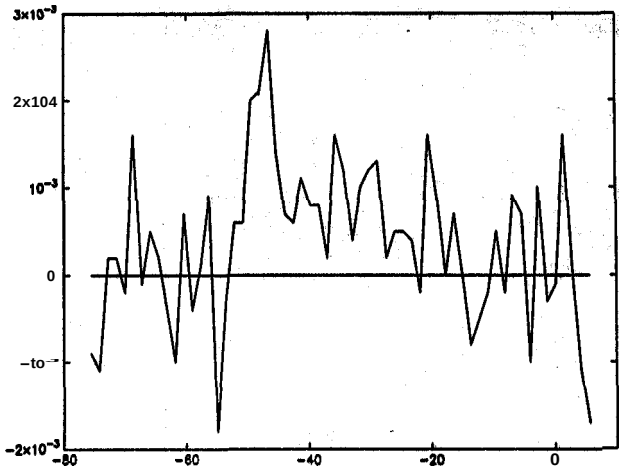

Figure 3.24 C270α spectrum integrated over Cas A

The continuum image of Cas A at 330 MHz with a beam of 27" × 21" (PA = -79°) is shown in Fig 3.23. The shell-like morphology of Cas A is clearly seen. The continuum structure shown in Fig 3.23 consists of knots of emission and the brightest region occurs in the west of the source. The integrated continuum flux density of Cas A is 6050 Jy which is about 5.4 % higher than that estimated by Baars *et.al.* (1977). This excess flux is an artifact of the errors in the correction of the digitally measured visibility function (Bieging *et.al.* 1991) which occurs in the VLA correlator system for strong sources like Cas A. This error is likely to be smaller in the optical depth maps of the recombination lines which are formed from the ratio of the line to continuum strengths. The observed peak continuum and peak line brightness are 145 Jy/beam and 0.7 Jy/beam respectively. The rms noise on the continuum image is 375 mJy/beam and on the line image, the rms noise is 35 mJy/beam.

The spectrum in units of the source-integrated optical depth (τ which is equal to $\ln(\frac{S_l}{S_c} + 1) \sim S_l/S_c$ since $\frac{S_l}{S_c} << 1$) is shown in Fig 3.24. The line emission over the continuum source is integrated and then divided by the integrated continuum emission to obtain τ. One of the Perseus arm components at -47 kms^{-1} of amplitude 2.5 x 10^{-3} and width 5 kms^{-1} is clearly seen in the spectrum. The second Perseus arm component near -38 kms^{-1} and the Orion arm component seen in other observations (PAE89) are not detected. The rms noise in the spectrum is $\sim$ 7 x 10^{-4}. Since the spectral feature appearing near -38 kms^{-1} is of the order of 9 x 10^{-4} (Anantharamaiah *et.al.* 1994), and that near 0 kms^{-1} is close to 1 x 10^{-3} (Anantharamaiah *et.al.* 1994), these features are probably hidden in the noise in the spectrum shown in Fig 3.24.

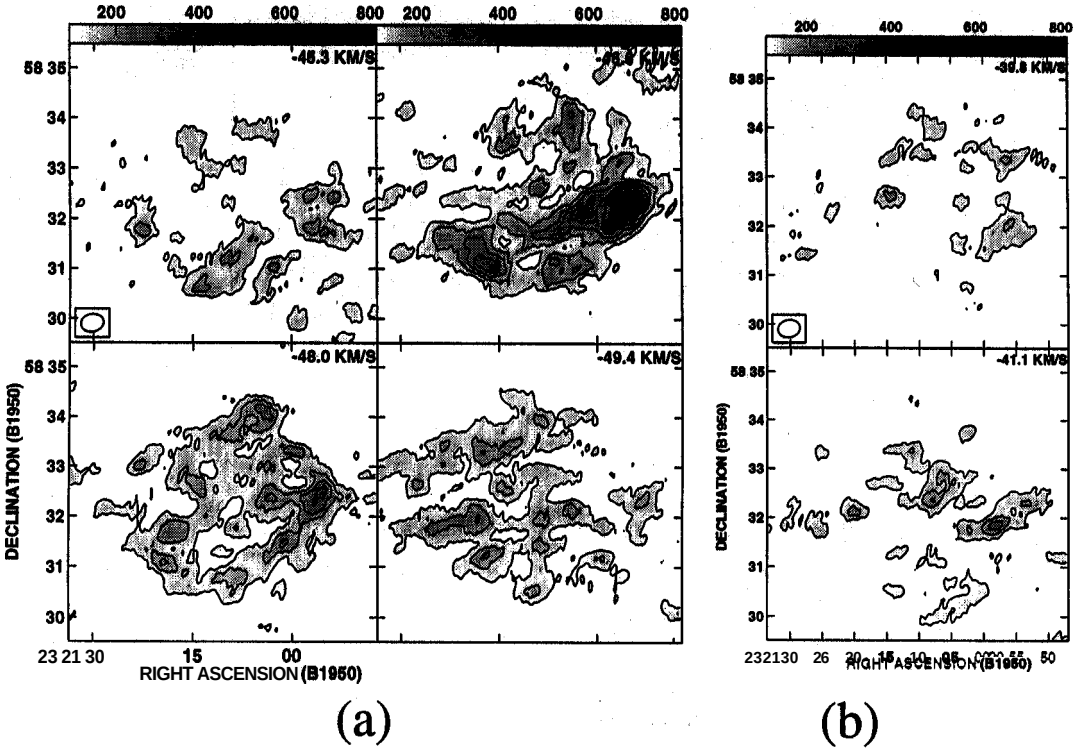

Figure 3.25 The distribution of C270α line emission across Cas A at different radial velocities corresponding to the Perseus arm. The beam (27"×21" with PA=-79') is shown at the bottom-left corner of the first panel of both the figures. The contour levels are 3,5,7,9,11,15 in units of 0.035 Jy/beam and the grey scale flux range is 0.1 to 0.8 Jy/beam. In (a), the line emission at -45.3, -46.0, -48.0 and -49.4 kms^{-1} is shown. In (b) the line emission at -39.8 and -41.1 kms^{-1} are shown.

The observed C270α line emission across Cas A at different radial velocities (-39.8 to -49.4 kms^{-1}) is shown in separate panels in Fig 3.25(a) & (b). Line emission observed over regions where the continuum source is stronger than 10 Jy/beam is shown in the figures. The different images are separated in velocity by 1.4 kms^{-1}. The strongest line emission is observed at -46.6 kms^{-1}. The line emission is patchy and the regions of bright line emission coincide with the continuum maxima. The morphology traced by the line emission resembles the continuum morphology, particularly in the southern and western regions. This is direct evidence of stimulated emission because the continuum emission is from the non-thermal emission of the supernova remnant whereas the recombination line emission arises in the foreground thermal gas. The observed line emission at other velocities is weak but wherever it is detectable, it coincides with the continuum maxima. The peaks of line emission seem to be drifting over the Cas A disk with change in the radial velocity. At -46.6 kms^{-1}, the western and southern parts of

Cas A emit strong line emission which becomes weaker at -49.4 kms^{-1}, but appears to be spread out in patches over almost the entire continuum disk. Weak emission is observed at velocities of -39.8 kms^{-1} and -41.1 kms^{-1}. These are the highest resolution recombination line images of Cas A at this frequency.

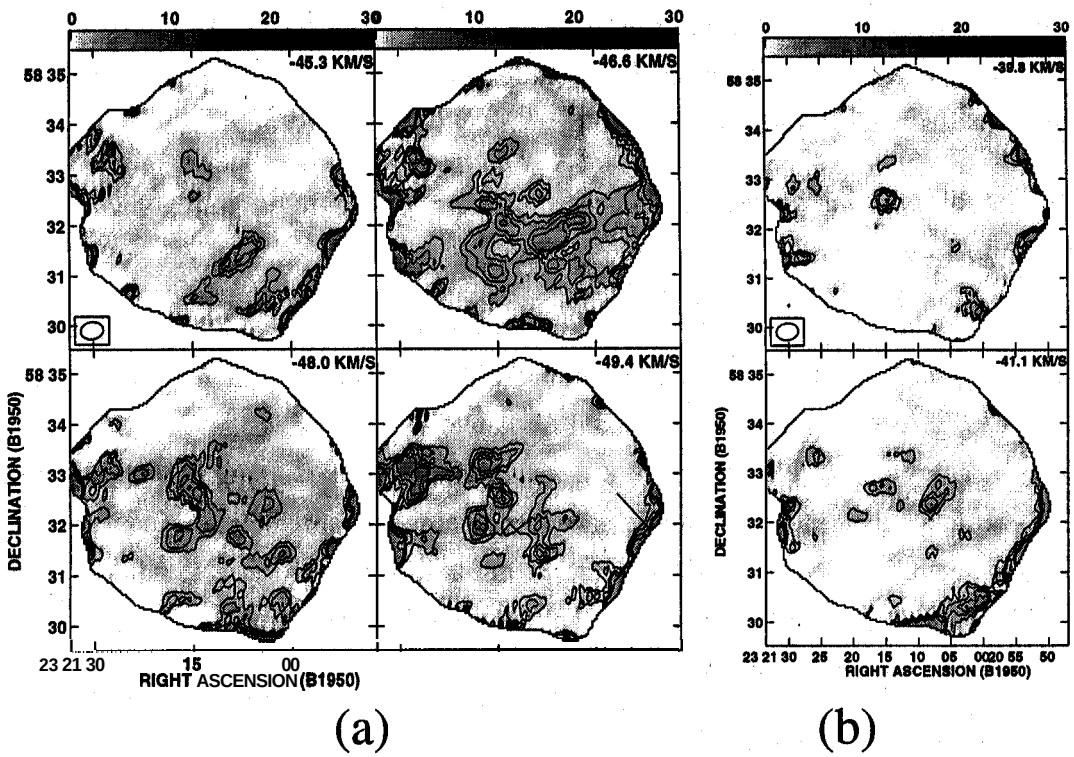

Figure 3.26 The distribution of C270α optical depths across Cas A at radial velocities where line emission is detected. The beamsize (27" x 21" with PA $= -79°$) is depicted in the bottom left corner of the first panel of both the figures. The contour levels are 3,4,5,6 in units of 0.001 Jy/beam and the grey scale flux range is from 0 to 0.03 Jy/beam. In (a), the distribution at velocities –45.3, –46.0, –48.0 and –49.4 kms^{-1} is shown. In (b), the distribution is shown for –39.8 and –41.1 kms^{-1}.

In Fig 3.26 (a) & (b), the optical depth images obtained from the line and continuum images of Cas A are shown. The optical depth at each point in the image is calculated from the quantity $\ln\left(\frac{S_l}{S_c} + 1\right)$ using the task COMB in AIPS. The resolution of these images is 27" x 21". Interestingly, the largest optical depths are seen from the central parts of the continuum source which are not coincident with the continuum maxima. Comparison of these images with the distribution of the HI 21-cm line and the molecular lines at comparable spatial and spectral resolutions across Cas A would be useful in establishing the association between the ionized gas and neutral gas in the Perseus arm. This is discussed in Chapter 4.

3.5 Observations with the RRI 10.4 m Telescope

3.5.1 The Astrophysical Plan

The distribution of molecular hydrogen across Cas A ($\alpha_{1950} = 23^h21^m11^s$, $\delta_{1950} = 58°32'20"$) required for comparison with the spatial distribution of ionized carbon gas as discussed in Section 3.4 was obtained by mapping the ^{12}CO ($J = 1 \rightarrow 0$, 115.27 GHz) line emission with an angular resolution of 1' using the 10.4 m telescope of the Raman Research Institute at Bangalore.

3.5.2 Observations & Results

The Telescope

The 10.4m diameter millimetre wave radio telescope is located inside the RRI campus in Bangalore. The telescope has an altitude-azimuth mount with the receiver at the Nasymth focus and operates over radio frequencies in the range 80-116 GHz. In the receiver, the first stage converts the RF to an IF of 1.5 GHz using a Schottky mixer. This is then converted to 400 MHz in the second stage before detection in the backend. The spectrometer used was a 256-channel filter bank which gave a spectral resolution of 250 kHz (0.65 kms^{-1}). The typical double side-band system temperature during these observations was in the range of 1200-1800 K.

Observing Details and Data Analysis

A 13' x 13' region centred on Cas A was mapped in the ^{12}CO line at 115.27 GHz ($\lambda \sim 2.6mm$) in two sessions: March 1991 and April-May 1993. The angular resolution was $\sim$ 1' and the grid spacing was 1' in declination and 0.5' in the right ascension. The pointing accuracy was about 10". A chopper wheel with a room temperature absorber was used to calibrate the antenna temperature and to correct for atmospheric absorption. Owing to the Perseus and Orion arm components separated in velocity by nearly 50 kms^{-1}, we had to switch frequency by almost half the observing band. The data towards each position in the grid were recorded in the frequency-switched (every 2 sec) mode. Since frequency switching alone was unable to correct for the frequency response, a frequency-switched reference spectrum on an off-source position

was also obtained. Both, the on-source and off-source frequency-switched spectra were folded to obtain the spectra shown in Fig 3.27. The resulting difference spectrum between the on-source and reference positions, after the removal of a linear baseline is shown in Fig 3.28. This calibration using two switching techniques (frequency & position) was a compromise between an increase in the telescope time and good baselines.

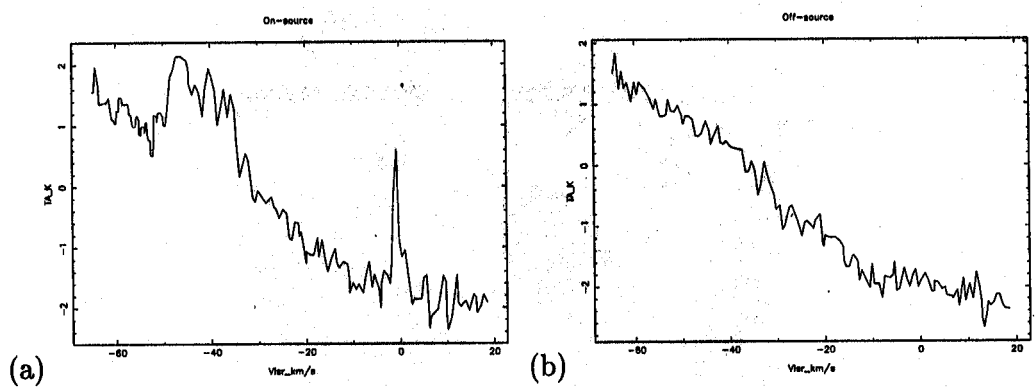

Figure 3.27 Frequency-switched ^{12}CO Spectrum towards Cas A after folding. The spectrum in (a) is obtained towards Cas A whereas the spectrum shown in (b) is obtained towards an offsource sky position. Notice that both show similar baseline variations.

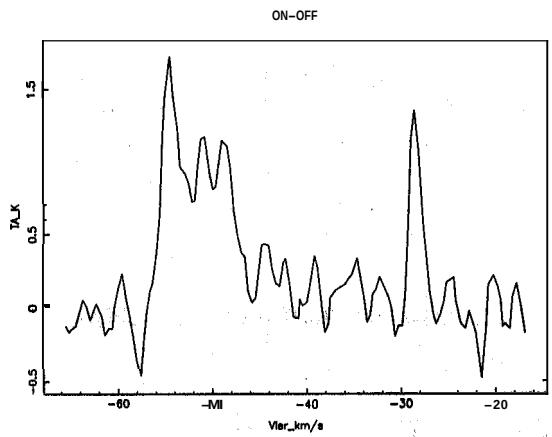

Figure 3.28 ^{12}CO emission over Cas A - Frequency-switched and Position-switched spectrum. To obtain this spectrum, the offsource frequency-switched spectrum is subtracted from the onsource frequency-switched spectrum. A linear baseline has then been removed from the spectrum.

The baseline variations were found to be fairly stable over time and the same off-source spectrum could be used for more than one pointing towards Cas A, thus reducing the total telescope time spent on the off-source positions.

The data were acquired and converted to the scan format of the NRAO single-dish spectral line data reduction package, POPS. The difference spectra were obtained from the position-switched data and then "folded". These spectra were visually examined for any problems. All the spectra corresponding to the 13'×13' region centred on Cas A were then converted to the FITS format and processed further using AIPS.

A typical spectrum from a pointing on Cas A is shown in Fig 3.28. The rms noise in all the spectra was ~ 0.3 K. The two Perseus arm components at velocities of about

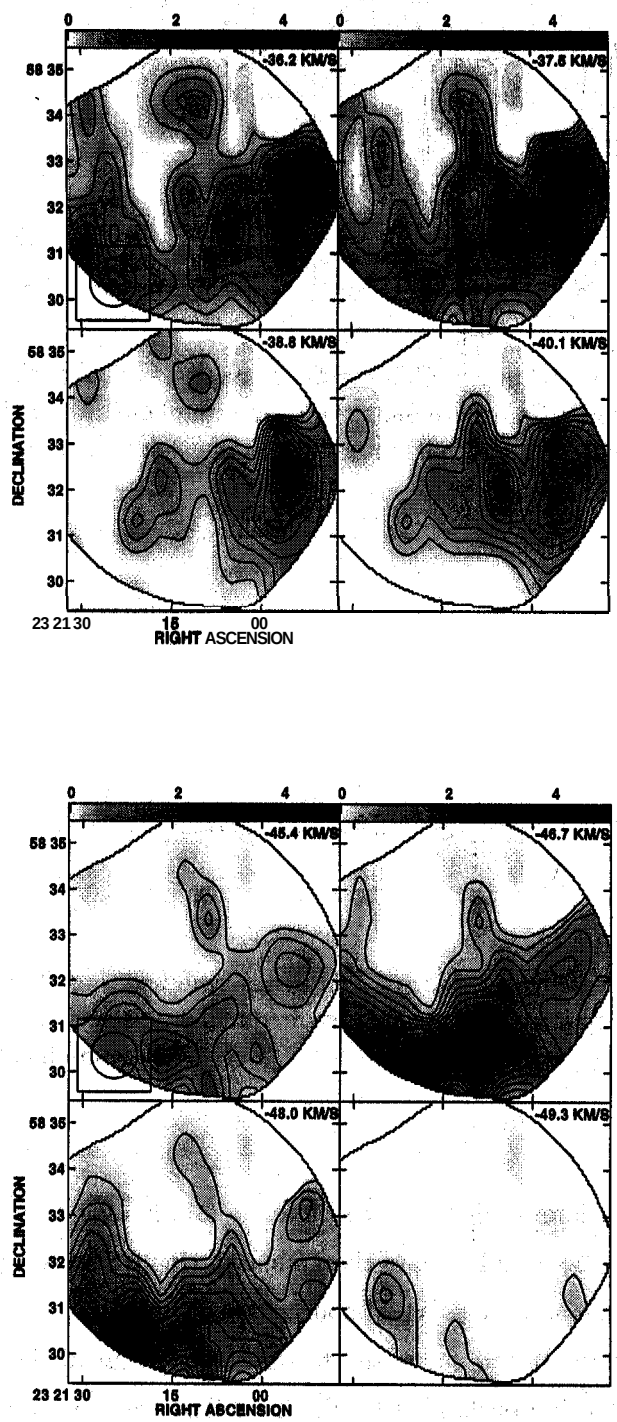

Figure 3.29 Distribution of ^{12}CO across Cas A. The grey scale flux ranges from 0 to 5 K. The contour levels are 1,2,3,4,5,6,7,8,9,10,11,13,15 plotted for every 0.3 K. The different panels show the distribution for different velocities which are shown in the top right corner. The beam used in the observations is shown in the lower left corner.

-38 kms^{-1} and -47 kms^{-1} are seen in spectra at all the grid positions. The Orion arm component appearing near 1.5 kms^{-1} is also clearly seen in the spectrum and is also found to be present over the entire continuum disk.

The distribution of ^{12}CO at different velocities is shown in separate panels of Fig 3.29. The distribution of molecular gas is found to vary with radial velocity.

The line emission from the gas in the Perseus arm is confined mostly to the south and west of the continuum source. In the velocity range of -35.5 to -40.0 kms^{-1}, the emission from the molecular gas peaks in the western part of Cas A and there is low-brightness emission' over the entire source. In the case of the gas appearing in the velocity range of -45.2 to -47.8 kms^{-1}, the emission is mainly confined to the southern parts of the continuum source. Strong ^{12}CO emission from the Orion arm is also observed. However these maps are not shown here.

The results of the comparision of these maps with that of the C270α and HI maps are presented in Chapter 4.

3.6 Summary

In this chapter, the telescopes that were used for the observations, the observations and their results have been described. The purpose of the observation, details of the telescopes, the HPBWs, observing frequencies and results are summarized in Table 3.8. The overall aim of all these observations was to understand the distribution and physical properties of the ionized carbon gas in the Galactic plane. In the next two chapters the interpretation of these results is presented.

Table 3.8 **Summary of various Observations made**

No.	Telescope	Observing Frequency (MHz)	Type of Observation	HPBW (EW x NS)	**Line(s)** Observed	Purpose	Results
1	Gauribidanur Radio Telescope	34.5	Single-dish	21' x **25°**	**C571α-C580α**	Observe lines in absorption from the Galactic Plane. and towards Cas A.	Lines detected at longitudes $l < 17''$ and a few other positions. Profile with Lorentzian wings detected in the spectrum towards Cas A.
2	Ooty Radio Telescope (Full)	326.5	Single-dish	2'' x 6'	H & C **270α-273α**	Observe lines in emission from the Galactic Plane. and towards Cas A.	Broad carbon lines detected from longitudes $l < 17''$ and a narrow line towards Cas A.
3	Ooty Radio Telescope (Single module)	326.5	Single-dish	2'' × 2''	H & C **270α-273α**	Observe emission lines with a larger beam	Carbon lines detected from $l < 17''$ with strengths similar to lines from the full telescope.
4	Very Large Array (D-array) NM, USA	332	Interferometric	5.3' x 3.3'	H & C **270α,271α**	Image ionized gas towards **G14+00** using recombination line emission.	No carbon line emission **upto** a 3σ limit of 60 **mJy/beam**. H line detected.
5	Very Large Array (B-array) NM, USA	332	Interferometric	27'' x 21''	H & C 270a	Image the ionized gas towards Cas A using recombination lines.	Detailed distribution of carbon line emission from the **gas** in **Perseus** arm across Cas A obtained.
6	RRI 10.4m Telescope, Bangalore	115270	Single-dish	**1'×1'**	^{12}CO (J=1-0)	Image the molecular gas towards Cas A.	Distribution of molecular gas towards Cas A obained.